1-1-2005

The Use of Compression Precracking Constant Amplitude (CPCA) Test Method to Obtain Near-Threshold Fatigue Crack Growth Behavior In AA7075-T7351

Dustin Henry McKnight

THE USE OF COMPRESSION PRECRACKING CONSTANT AMPLITUDE (CPCA) TEST METHOD TO OBTAIN NEAR-THRESHOLD FATIGUE CRACK GROWTH BEHAVIOR IN AA7075-T7351

By

Dustin Henry McKnight

A Thesis
Submitted to the Faculty of
Mississippi State University
in Partial Fulfillment of the Requirements
for the Degree of Master of Science
in Mechanical Engineering
in the Department of Mechanical Engineering

Mississippi State University

December 2005

THE USE OF COMPRESSION PRECRACKING CONSTANT AMPLITUDE (CPCA) TEST METHOD TO OBTAIN NEAR-THRESHOLD FATIGUE CRACK GROWTH BEHAVIOR IN AA7075-T7351

By

Dustin Henry McKnight

Approved:

Judith A. Schneider Associate Professor of Mechanical Engineering (Director of Thesis)	Steven Daniewicz Professor of Mechanical Engineering (Committee Member)
James C. Newman Jr. Professor of Aerospace Engineering (Committee Member)	Donald M. Smith Adjunct Professor of Civil Engineering (Committee Member)
Peter McKeighan Southwest Research Institute (Committee Member)	
Steven Daniewicz Graduate Coordinator of the Department of Mechanical Engineering	Roger King Associate Dean of Bagley College of Engineering

Name: Dustin Henry McKnight

Date of Degree: December 10, 1005

Institution: Mississippi State University

Major Field: Mechanical Engineering

Major Professor: Dr. Judith A. Schneider

Title of Study: THE USE OF COMPRESSION PRECRACKING CONSTANT AMPLITUDE (CPCA) TEST METHOD TO OBTAIN NEAR-THRESHOLD FATIGUE CRACK GROWTH BEHAVIOR IN AA7075-T7351

Pages in Study: 62

Candidate for Degree of Master of Science

Traditionally, pre-cracking has been performed under tension-tension loading, followed by a load reduction scheme to obtain fatigue crack growth rate data in the near threshold regime. These data have been shown to show load history effects due to remote crack closure. An alternative test method has been developed to minimize these load history effects. This test procedure uses compression pre-cracking to initiate a crack, followed by constant amplitude loading to grow the crack to failure. Compression-compression (C-C) loading as a means of forming a starter crack for fatigue crack growth is a relatively new concept. Cracks grown under C-C loading emanate from the notch tip due to a tensile residual stress field formed during the unloading cycle. The subsequent constant amplitude steady-state crack growth is free of load history effects, after crack growth beyond several compressive plastic zone sizes, and therefore will

give a better steady-state representation of the near-threshold regime. A more in-depth examination at this phenomenon is performed herein.

ACKNOWLEDGMENTS

The author would like to recognize those who have helped in the completion of this research. Foremost, the author wishes to thank Dr. Judy Schneider, for her continual support. Also, Dr. James Newman is acknowledged for his expertise and support in the lab and in doing research. The author would also like to thank his committee members Dr. Pete McKeighan, Dr. Don Smith, and Dr. Steven Daniewicz for their suggestions that have greatly improved this research. Finally, recognition is given for the funding provided by the Office of Naval Research (ONR Grant # N00014-02-1-0379).

TABLE OF CONTENTS

LIST OF FIGURES

FIGURE Page

LIST OF TABLES

LIST OF ABBREVIATIONS AND SYMBOLS

a	Crack Length
A*	Compliance
AA	Aluminum Alloy
ASTM	American Society for Testing and Materials
B	Specimen Thickness
BFS	Back-Face Strain
C	K-Gradient Parameter
C-C	Compression-Compression
COD	Crack Opening Displacement
CPCA	Compression Precracking Constant Amplitude
C(T)	Compact Tension Specimen
DTD	Damage Tolerant Design
da/dN	Crack Growth Rate
ΔK	Stress Intensity Factor Range
ΔK_{apl}	Applied Stress Intensity Factor Range
ΔK_{eff}	Effective Stress Intensity Factor Range
ΔK_{th}	Threshold Stress Intensity Factor Range
$\Delta\sigma$	Stress Range
E	Elastic Modulus

ε	Strain
ESE(T)	Single Edge Crack Tension Specimen
F	Boundary Correction Factor
FCG	Fatigue Crack Growth
FCGR	Fatigue Crack Growth Rate
FTA	Fracture Technology Associates
ρ_c	Plastic Zone Size
JSC	Johnson Space Center
K	Stress Intensity Factor
K_{1c}	Plane-Strain Fracture Toughness
K_{max}	Maximum Stress Intensity Factor
K_{min}	Minimum Stress Intensity Factor
K_{op}	Crack-Opening Stress Intensity Factor
LR	Load Reduction
LA	Lab Air
M(T)	Middle-Crack Tension Specimen
NASA	National Aeronautics and Space Administration
OA	Over-aged
P_{min}	Minimum Load
P_{max}	Maximum Load
R	Load Ratio
ρ_c	Plastic Zone Size

RH	Relative Humidity
R_{SC}	Strength Ratio
RT	Room Temperature
S_{max}	Max Applied Stress
S-N curve	Stress-Life Curve
S_o	Crack-Opening Stress
σ_{ys}	Monotonic Yield Strength
UTS	Ultimate Tensile Strength
W	Specimen Width

CHAPTER I

INTRODUCTION

Understanding fatigue crack growth thresholds is a fundamental step in evaluating service life of structural components. Therefore obtaining an accurate threshold behavior for crack growth is essential. Current testing procedures for fatigue crack growth thresholds are outlined in ASTM Standard E647-00. The procedure involves gradually decreasing load until the subsequent fatigue crack growth rate is negligible. The threshold stress intensity range is a function of material, environment, and load ratio (P_{min}/P_{max}). There has been some concern though that this method results in higher apparent thresholds than steady state constant amplitude loading due to load history effects.

The current research studies a new test method that will minimize the load history effects observed in the near-threshold region. In this method a precrack is first grown under compression-compression loading transitioning later to constant amplitude loading. It is this compression-compression constant amplitude test method that is the subject of the current research.

1.1 Background

Fatigue first became a major concern in the 1840's with the failure of railroad axles. Axles were failing at shoulders due to what became known as fatigue. In the 1950's several Comets, the first jet propelled passenger planes, crashed due to repeated cabin pressurizations. More recently, in 1988, Aloha Airlines flight 243 lost the top half of its fuselage due to multiple fatigue cracks emanating from rivet holes. Each of these catastrophic events sparked extensive studies into fatigue and fatigue crack growth[1].

When designing for fatigue life, design engineers select from four criteria: Infinite-life design, safe-life design, fail-safe design, and damage tolerant design. A part is designed for infinite-life by limiting the stress amplitude below an endurance limit. The endurance limit is an upper limit for stress amplitude below which a crack will not nucleate after 10^7 cycles. In safe-life design a design engineer uses S-N curves to determine the maximum number of cycles a part can withstand at a prescribed stress level before crack initiation and then adds a safety factor to account for variability. In safe-life design the component is taken out of service when the cyclic life of a component is met. Fail-safe design takes precautions with redundant load paths to protect a system as a whole by allowing the failure of one part to not affect the entire system. Damage tolerant design (DTD) assumes that cracks exist and uses analysis, testing, and inspection to safely manage fleet cracking. Use of DTD is increasing in industry because of the recognition that cracks eventually initiate in components under cyclic loading

and the part will have a finite life as the crack grows. Use of DTD is a more financially practical alternative to taking the part out of service every time a crack is detected. However, in order to implement DTD, it is necessary to understand how the stresses imposed on the part or component affect the fatigue life of a crack, or crack growth rate, and thus the operable service life of the part or component. Of particular concern is the stress intensity level at which a crack starts to grow, or the threshold stress intensity range.

1.2 Fatigue Crack Growth Life

To understand the life of a cracked component the stress intensity range, ΔK, was introduced and compared to the rate of crack growth, da/dN [2]. The stress intensity range can be applied to either one of the three Modes of loading, shown in Figure 1.

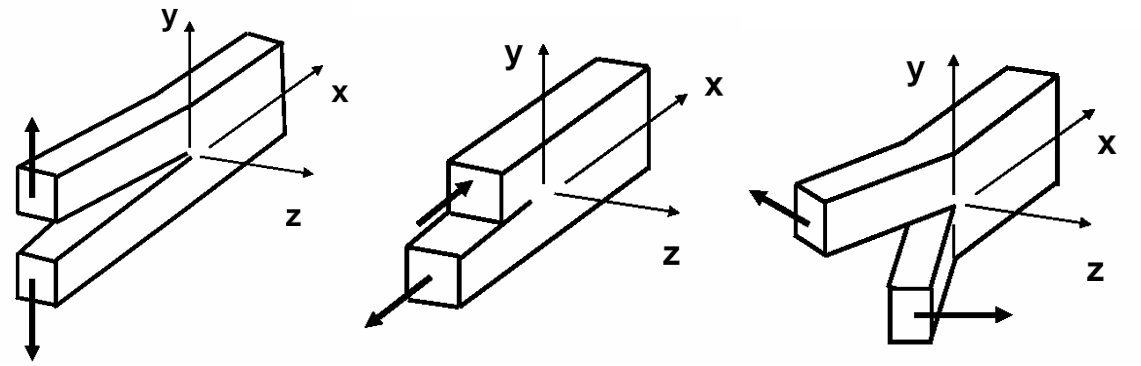

(a) (b) (c)

Figure 1: Three modes of specimen loading; a) Mode I, b) Mode II, c) Mode III [3]

The three modes of loading are: Mode I loading, Figure 1a, which is the most common type of loading and is simple tensile loading, Mode II loading, Figure 1b, which is a shear type of loading, and finally Mode III which is an out of plane loading shown in Figure 1c. The Mode I, ΔK will be used exclusively throughout this research

ΔK, given by equation 1, is function of the applied stress, crack length and specimen geometry,

$$\Delta K = \Delta\sigma\sqrt{\pi a}\, f(a/W) \tag{1}$$

where Δσ is the change in stress, a is the crack length, and f(a/W) is a function of the specimen geometry. The crack growth rate, da/dN, is the incremental rate of change in crack length divided by the incremental rate of change in cycles. The relation between ΔK and da/dN can be plotted on a fatigue crack growth (FCG) curve, shown in Figure 2. The FCG curve is plotted on a log-log scale which results in a sigmoidal shape. Since ΔK is a function of the applied load, specimen geometry, and crack length, it is possible to relate laboratory data to real-life components in what is referred to as similitude [1].

As illustrated in Figure 2, there are three regions in the FCG curve: the threshold region, the Paris regime, and the fracture region. The linear Paris regime is named after Paul Paris who first related crack growth rate to ΔK [2] defined by equation 2,

$$\frac{da}{dN} = A(\Delta K)^n \tag{2}$$

where A is the coefficient found by extending the straight line to $\Delta K = 1$ ksi-in$^{1/2}$ and n is the slope of the line in log-log space. A is a function of the load ratio and stress level.

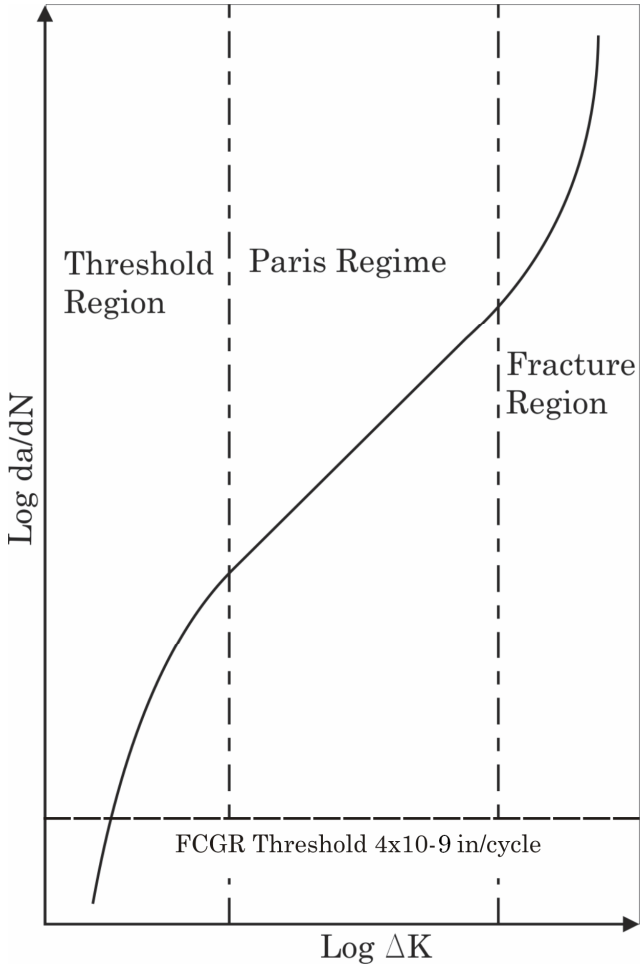

Figure 2: Typical fatigue crack growth curve plotting ΔK versus da/dN

The far right hand side of the FCG curve is the fracture region where the crack experiences accelerated crack growth and approaches a critical stress intensity. Conversely, on the far left hand side of the FCG plot, the crack growth decelerates as it enters the threshold region and approaches the threshold stress

intensity range. The threshold stress intensity range for FCG has been defined by ASTM as the stress level at the crack growth rate of 10^{-10} m/cycle [4] which corresponds to, at 1 hertz cyclic frequency, a crack growth of approximately 10 mils in 30 days. Cracks growing in this slow growth rate regime are considered to be less critical.

Fatigue crack growth takes place in two distinct stages: Stage I growth and Stage II growth. Stage I takes place when the crack tip follows along the crystallographic plane upon which slip occurs. A variation in crack path occurs due to underaging (Fig. 3a) and overaging (Fig. 3b) of 7475 AA in Figure 3. Stage II is the subsequent growth when the crack plane lies normal to the applied. Where Stage I is normally correlated with crack initiation, the growth of small fatigue cracks, and at low crack growth rates, Stage II is the most commonly observed stage of fatigue crack growth.

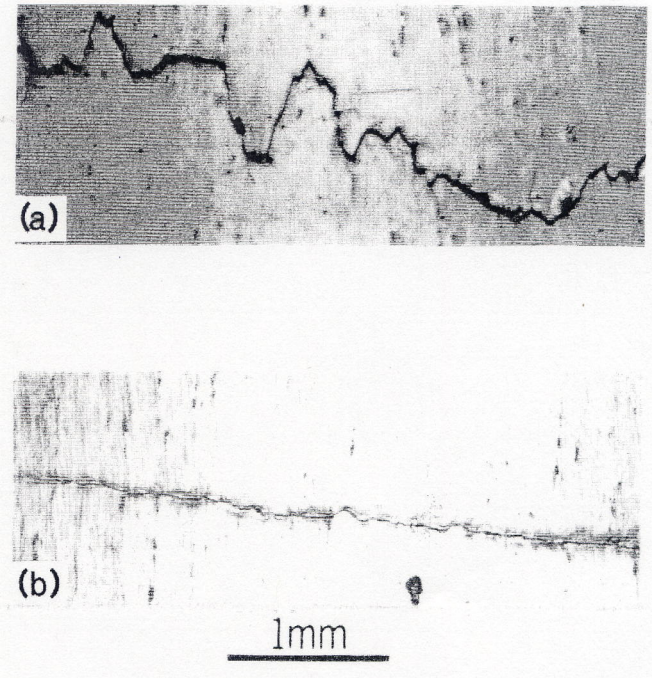

Figure 3: Optical micrograph showing the crack paths of 7475 tested in vacuum; a) under-aged condition, Stage I growth, b) over-aged condition, Stage II growth [5]

The objective of this research project is the investigation of long crack growth in the near threshold region of the crack growth rate curve. A new procedure using compression precracked, constant amplitude, steady-state testing to measure near threshold rate behavior was focused on.

1.3 Fatigue Crack Growth Threshold Testing Methods

The industry standard used for fatigue crack growth tests is ASTM E647-00 [4] and is comprised of three types of tests: constant amplitude, load reduction, and K_{max} testing.

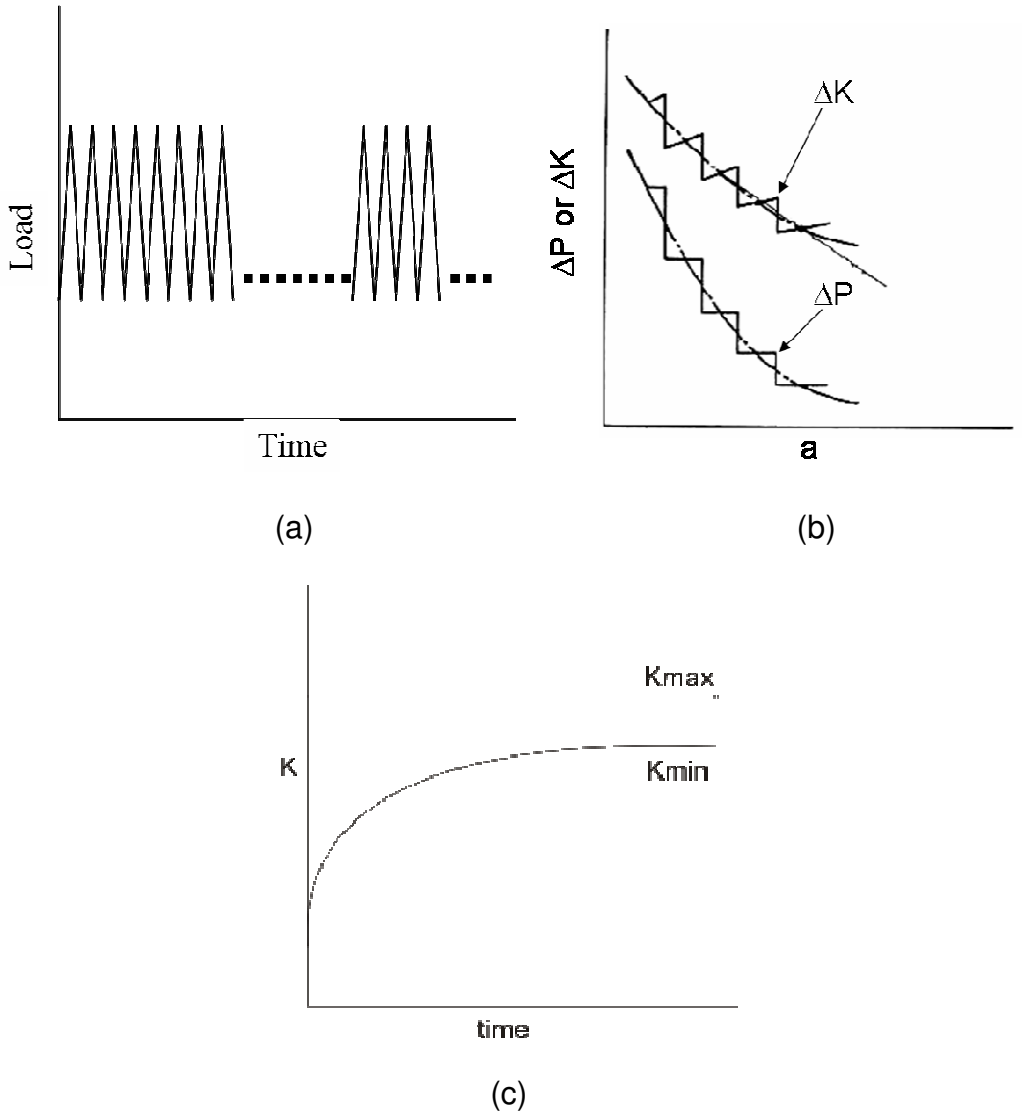

Figure 4: Three fatigue crack growth test methods a) Constant Amplitude, b) Load Reduction, c) Constant K_{max}

Illustrated in Figure 4a is constant amplitude testing in which the minimum and maximum loads are held constant during the test duration, thus as the crack grows, the ΔK value increases. Shown in Figure 4b is the load reduction method in which the ΔK value is incrementally reduced by decreasing the load at a step

rate, C, as the crack grows. The rate at which the load is dropped is called the K gradient and is defined by equation 3,

$$C = (K^{-1})*(dK/da) > -0.08\ mm^{-1}\ (-2\ in^{-1}) \quad (3)$$

Where K is the stress intensity, and dK/da is the incremental change in stress intensity over the incremental change in crack length. In both the constant amplitude and load reduction methods the load ratio of P_{min}/P_{max} is held constant. In contrast the K_{max} test varies load ratio by holding K_{max} constant while increasing K_{min}, which is illustrated in Figure 4c. For crack growth rates greater than 10^{-8} m/cycle, the ASTM E647-00 Standard recommends the use of constant amplitude testing and for crack growth rates less than 10^{-8} m/cycle the load reduction method is recommended. The K_{max} test can yield threshold data but only at a high load ratio of R>0.9. Therefore, according to ASTM E647-00, to obtain the threshold stress intensity range at various load ratios the load reduction method is recommended.

The reasoning behind the recommendation of the load reduction test for threshold testing, as opposed to constant amplitude testing, concerns notch tip issues created during pre-cracking. Prior to performing fatigue crack growth tests a pre-crack must be made to ensure a sharp crack and to ensure sufficient growth away from notch radius effects. Because ΔK_{th} defines the stress intensity level below which a crack does not grow, it is therefore impractical to grow a crack from the notch tip at or below ΔK_{th}. Always in fatigue crack growth testing, the pre-crack is grown above the threshold value, and after a suitably long crack

is grown, the load reduction method is performed to generate the threshold region of the growth rate curve. Recommendations for generating a pre-crack are provided in ASTM E647-00 and include the following requirements:

1. The pre-crack must be greater than or equal to 10% the specimen thickness (B) or 0.04 in, whichever is smaller.
2. The K_{max} for pre-cracking cannot exceed the K_{max} for testing.
3. Crack sizes on the front and back surfaces cannot differ by more than 25% of the specimen thickness (B).

Although accurate determination of threshold is important in fatigue life prediction, it is difficult to obtain unique values in controlled laboratory environments. Several confounding factors affect the uniqueness of an accurate threshold value: plasticity [6-8], surface oxidation or environment [9], mismatching of the fracture surface [10], load ratio [7, 11], initial stress levels [7, 11], specimen type [12, 13], and specimen size [13, 14]. These confounding factors cited often result in variations in the reported threshold value for a particular metal or alloy. Many of these various factors affect the growth of a crack by interfering with the closing of the crack face and are usually expressed by the term closure.

1.4 Effect of Crack Closure on Growth Rate

Fatigue crack closure is defined as the premature closing of the crack face prior to complete unloading. This is a primary concern at low R values, where

there is a greater opening of the crack surface, and has been reported to be caused by the following three mechanisms [6-10]:

1. Crack tip plasticity
2. Fracture surface oxidation
3. Fracture surface roughness

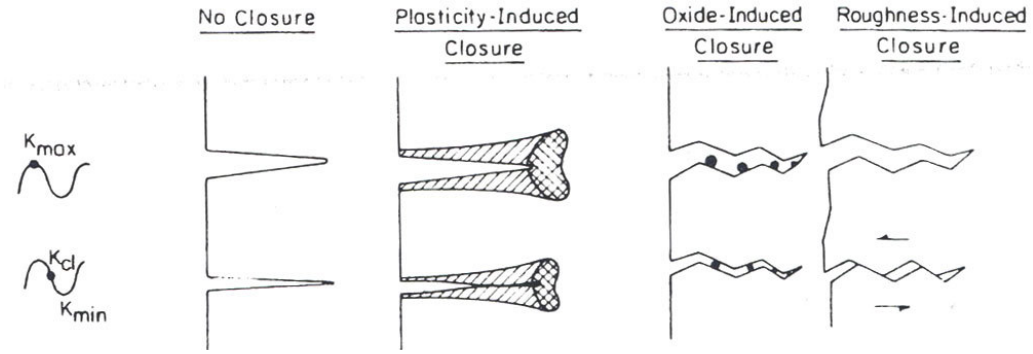

Figure 5: Mechanisms of fatigue crack closure [10]

ASTM standard E647-00, section 5.1.6 has the following statement regarding fatigue crack closure:

> Crack closure can have a dominant influence on fatigue crack growth rate behavior, particularly in the near-threshold regime at low load ratios. This implies that the conditions in the wake of the crack and prior loading history can have a bearing on the current propagation rates. The understanding of the role of the closure process is essential to such phenomena as the behavior of small cracks and the transient crack growth rate behavior during variable amplitude loading. Closure provides a mechanism whereby the cyclic stress intensity near the crack tip, ΔK_{eff} differs from the nominally applied values, ΔK. This concept is of importance to the fracture mechanics interpretation of fatigue crack growth rate data since it implies a non-unique growth rate dependence in terms of ΔK and load ratio [4].

The premature closing of the crack face can result in a reduction of the ΔK applied at the crack tip. This is important since crack advance can only occur when the crack is open. The reduced stress intensity range at the crack tip is called ΔK_{eff}. This reduction in ΔK is mostly observed at load ratios less than 0.6. The equations used for ΔK_{eff} are given in equation 4 and 5,

$$\Delta K_{eff} = K_{max} - K_{op} < \Delta K_{apl}; \quad \text{if } K_{op} > K_{min} \tag{4}$$

$$\Delta K_{eff} = \Delta K_{apl} = K_{max} - K_{min}; \quad \text{if } K_{op} \leq K_{min} \tag{5}$$

Where K_{max} is the max applied stress intensity, K_{min} is the minimum applied stress intensity, K_{op} is the opening stress intensity, and ΔK_{apl} is the applied stress intensity factor range. Closure caused by crack tip plasticity was first recognized by Elber in 1970 [6]. His conclusions suggested that the plastic deformation of the material at the crack tip could result in incompatible mating surfaces when confined by the non-deformed material surrounding the plastic zone. This phenomenon is generally observed in plane stress, thin gage specimens.

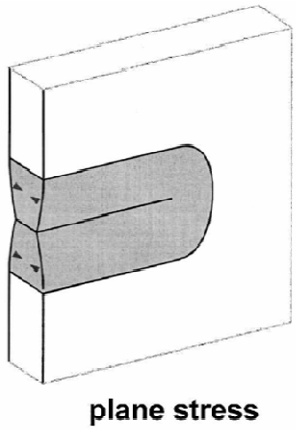

Figure 6: Plasticity effects in a plane stress specimen [15]

Necking of the sides of a plane stress specimen due to loading is illustrated in Figure 6. Varying degrees of necking can be observed depending on the magnitude of the applied load. This necking effect causes the mismatches between the two crack fracture surfaces.

Following Elber's pioneering research other mechanisms of crack closure have been introduced based on crack surface corrosion deposits, or oxide-induced closure [9], and crack surface roughness, or roughness-induced closure [10].

Oxide induced closure occurs when a layer of oxidation forms on fresh fracture surface in the crack wake and prevents the crack from fully closing during unloading. Surface-roughness induced closure is illustrated in Figure 3 and is a result of two effects. The first effect is when the crack tip plastic zone is smaller than the grain diameter, which results in stage I type crack growth. The second is the addition of mode II type loading. The tortuous crack growth and mixed mode loading causes incompatible fracture surfaces. Various researchers [5, 8, 10] have shown that roughness-induced closure is most common in the low crack growth rate regimes near threshold.

Other effects observed in fatigue crack growth can be attributed to plasticity induced closure. Effects due to geometry differences, differences in size, load ratio, starting ΔK, and load shed rate can lead to variations in threshold stress intensity values.

Conventionally fatigue has been characterized by a single parameter, ΔK. By using the stress intensity factor range it is possible to apply data taken from a laboratory specimen to data taken from full scale testing. The stress intensity range correlates data from various geometries to one unifying parameter. Thus, material properties such as ΔK_{th} will not vary due to specimen geometry or size. This fundamental assumption of fracture mechanics is termed similitude.

Recent research has shown that this assumption is not always valid. Tests performed by Garr and Hresko on Inconel-718 [14] are illustrated in Figure 7. Compact tension specimens of widths of 2 and 5 inches were used for testing. The data illustrate that there are distinct differences in the fatigue crack growth curves for the two widths. At a load ratio of 0.7 the two curves begin to deviate at a crack growth rate of 10^{-6} mm/cycle. For a load ratio of 0.1 the curves separate at a higher growth rate of 10^{-3} mm/cycle. This leads to a difference in threshold of nearly 3 times.

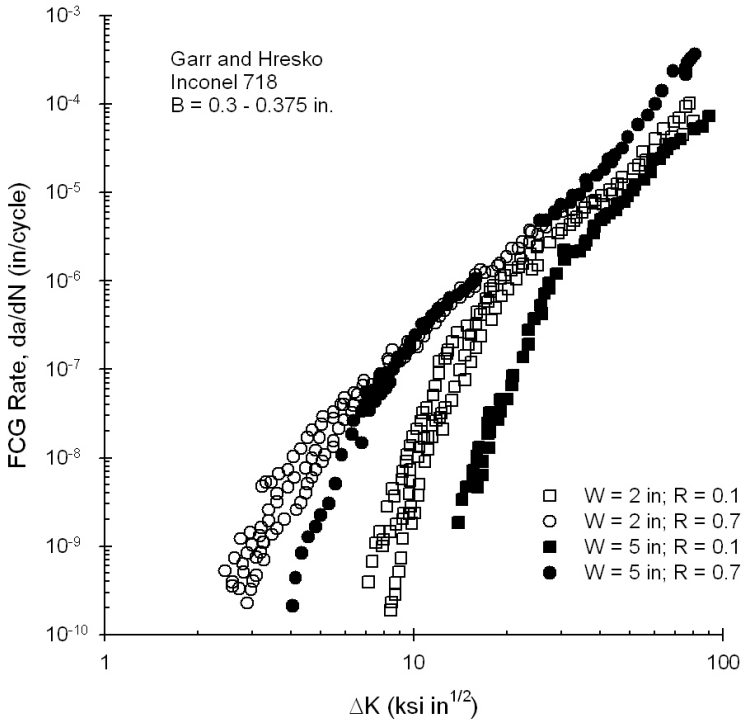

Figure 7: Fatigue crack growth differences due to specimen sizes in Inconel-718 [14]

Forth et al. [13] have studied the effects of geometry on fatigue crack growth. They compared 4340 steel fatigue crack growth curves for M(T) and C(T) specimens of similar thickness and width. The tests in Figure 8a were perform at a load ratio of 0.1. The C(T) specimen has a threshold stress intensity range of approximately 9 compared to the MT specimen that has a threshold stress intensity range of approximately 5. In Figure 8b, the load ratio of 0.5 curve for the MT specimen is to the left of the 0.7 curve for the C(T) specimen. Under normal steady state conditions the R of 0.5 should be to the right of the R of 0.7 curve.

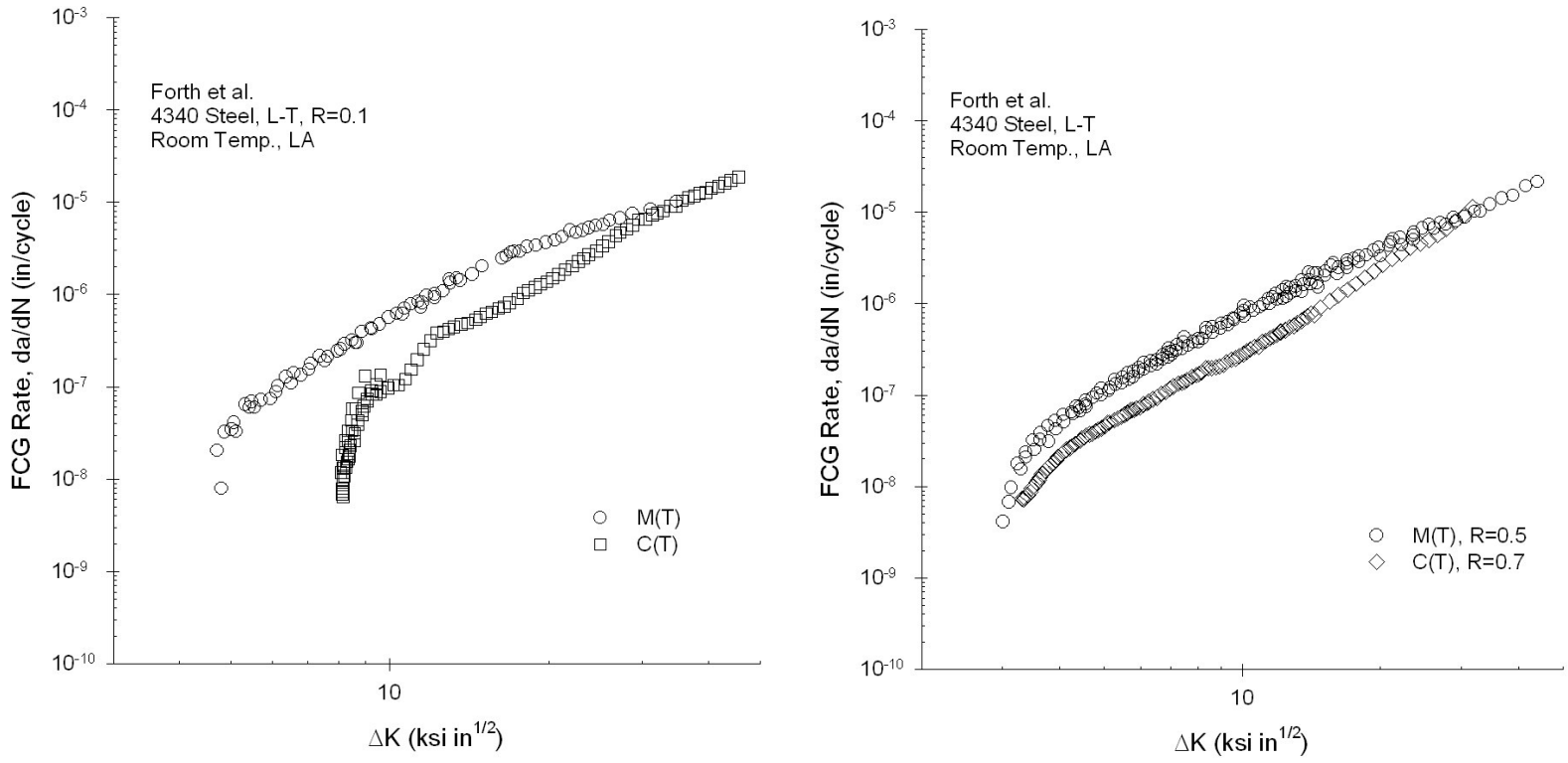

Figure 8: Fatigue crack growth differences due to specimen configuration, a) R = 0.1 conditions, b) R = 0.5 and 0.7conditions [13]

Tests at near threshold stress intensity values have shown differences due to differences in load ratios. It had been a point of contention between researchers whether the ASTM standard has a substantial effect on near-threshold values [7, 11, 16]. The test method has been shown to affect threshold values due to starting stress levels and load shed rates. These effects have been lumped together into what is known as "Load History Effects." These load history effects have caused a "fanning" effect of the fatigue crack growth data. The fanning effect at lower load ratios is shown in Figure 9. Lower load ratios have been shown to be more susceptible to plasticity induced closure. This is due to the large difference between maximum and minimum loads. With the larger load ratios the minimum loads are not low enough to be below K_{op} therefore there are no effects.

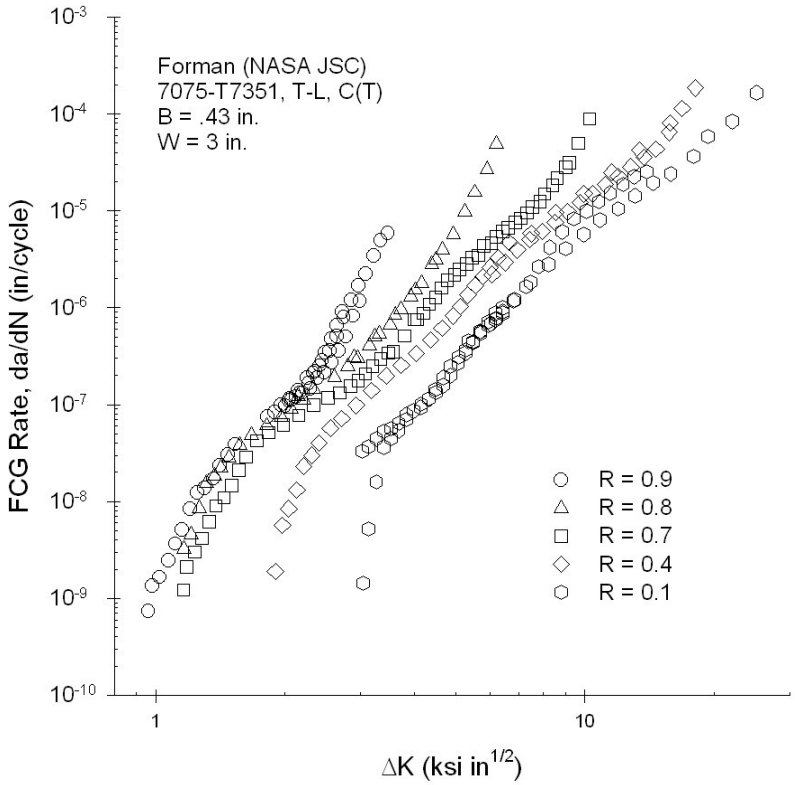

Figure 9: Fatigue crack growth differences in load ratio due to load history effects [17]

1.5 Effective Stress Intensity Factor Range

As discussed in Section 1.3, ΔK_{eff} is used to describe the stress applied at the crack tip due to closure. Elber developed the effective stress intensity factor equation,

$$\Delta K_{eff} = (S_{\max} - S_o)\sqrt{\pi \cdot a} \cdot F \tag{6}$$

where S_{max} is the max applied stress, S_o is the crack-opening stress, a is the crack length, and F is a boundary correction factor. Equation 6 can be modified to give the equation for any crack configuration,

$$\Delta K_{eff} = U \cdot \Delta K = [(1 - S_o / S_{\max}) / (1 - R)] \cdot \Delta K \tag{7}$$

Newman has developed equations for steady state crack-opening stress from the plasticity induce crack closure that take into effect load ratio and constraint factors, α. These equations have been incorporated into the FASTRAN model. The constraint factors are used to correlate the steady-state constant-amplitude conditions at the various load ratios in the mid-rate Paris regime. This will not however correlate the non-steady-state constant amplitude conditions in the near threshold region due to the many variables affecting FCGR thresholds [18, 19].

Using equation 7, and FASTRAN results for crack-opening stress, the FCG curves from Forman et al's research on 7075-T7351 [17] can be replotted showing the crack growth rate against ΔK_{eff}. Effective stress intensity results from Forman et al. is shown in Figure 10 with the effective stress intensity baseline shown as a solid line.

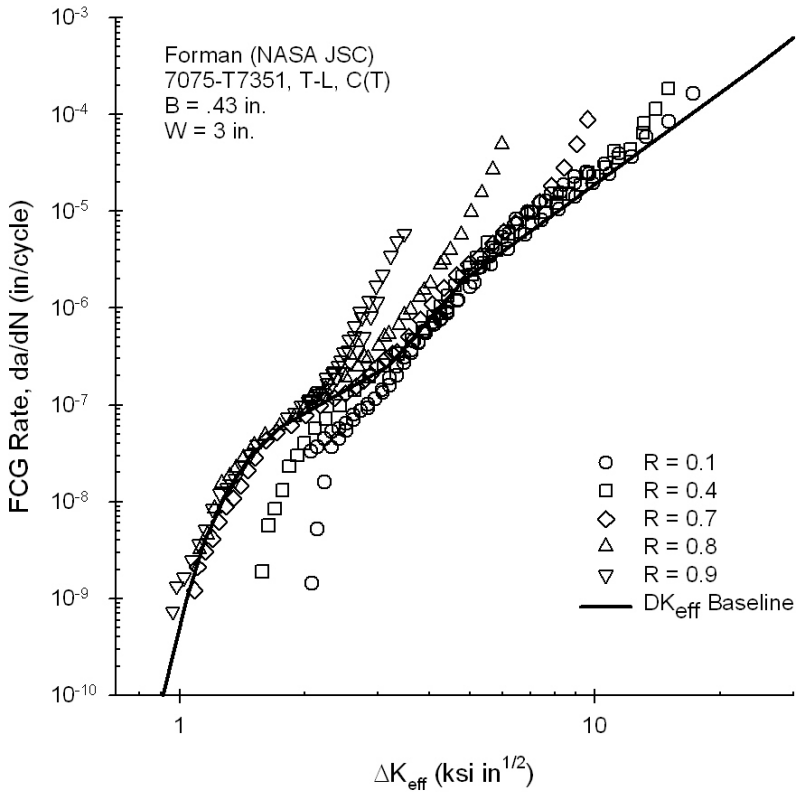

Figure 10: Combining fatigue crack growth curves using ΔK_{eff} [20]

The ΔK_{eff} curve is a tool to demonstrate the non-steady state FCG at the lower growth rates. The lower load ratios in Figure 10, demonstrate the results of the load reduction procedure on steady state crack growth.

Recently a new test method to determine fatigue thresholds has been proposed which uses compression pre-cracking [17, 21-24]. The use of compression pre-cracking allows for a fatigue test to be initiated at ΔK ranges below threshold. Following the compression-compression precracking, the fatigue crack growth test can be carried out under constant amplitude loading.

The advantage of this test method is that the near-threshold data are obtained by naturally increasing ΔK rather than decreasing ΔK. The illustration in Figure 11 compares the two test methods by showing the different paths for the fatigue crack growth curves for the two different test methods and for different starting stress intensities. The compression precracking constant amplitude test method is believed to minimize or eliminate the "load history effects" caused by the load decreasing test method.

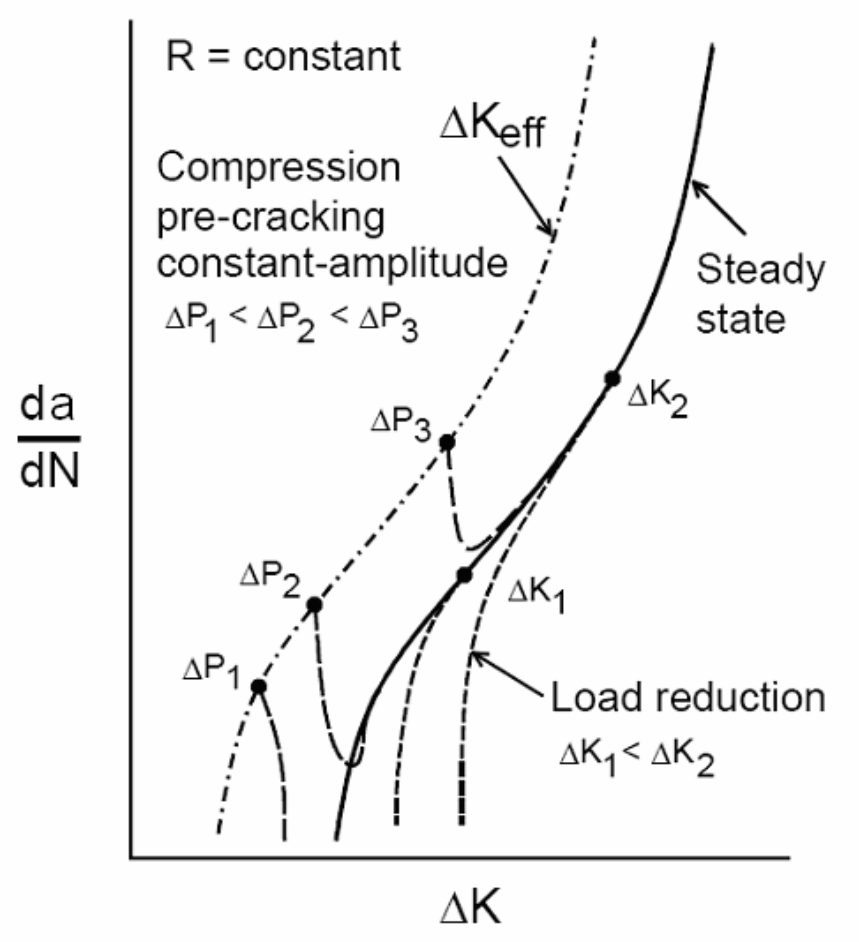

Figure 11: Fatigue crack growth plot comparing load reduction and compression compression constant amplitude test methods [20]

1.6 Compression Precracking

The use of compression-compression loading to grow a crack from a notch tip in metallic materials has largely been attributed to Hubbard from his 1969 paper, “Crack Growth Under Cyclic Compression [25].” Prior to this publication, it was widely assumed that a crack could not grow under cyclic compression and currently fatigue crack growth data from negative stress intensity range is generally ignored because it is assumed that these conditions do not contribute to crack extension. Hubbard [23] proposed that upon initial loading a compressive monotonic plastic zone is formed as illustrated in Figure 12a. Then during unloading a tensile cyclic plastic zone is formed. From the tensile cyclic plastic zone crack growth occurs. As the crack grows the monotonic plastic zone does not grow but the cyclic plastic zone keeps growing in progressively smaller increments until it reaches a threshold.

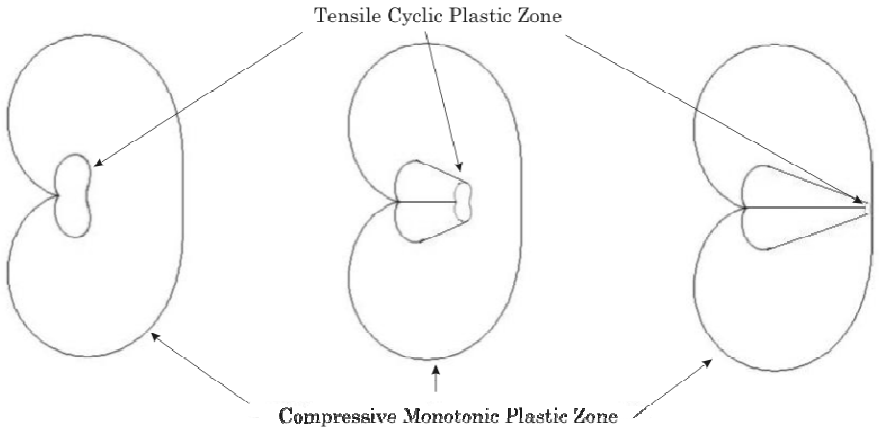

(a)

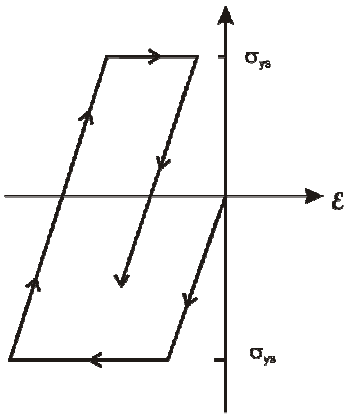

(b)

Figure 12: Fatigue crack growth under compression-compression loading

The cyclic stress-strain response is demonstrated in Figure 12b [26]. As the material is loaded in compression the material yields. Then as the material is unloaded reverse yielding occurs in tension. During the unload cycle the surrounding elastic material will relax due to the reduction in strain. The cyclic

plastic zone applies tensile residual stresses to the surrounding elastic material, which drives crack growth.

1.7 Compression-Compression Constant Amplitude (CPCA)

The use of compression-compression cracking was expanded to a means of obtaining a precrack for fatigue crack growth testing in the late 1980's by Suresh [22] and the in the early 1990's by Pippan [24]. Pippan proposed a step increase in load as crack extension occurs. Testing is initiated at loads below threshold. Loads are then increased at incremental rates until crack growth occurs. At a prescribed stress level the crack propagates and then stops. Pippan describes this stress level as the effective stress intensity threshold, $\Delta K_{th,eff}$. The load is then stepped up again until crack extension resumes. At this point the load is kept constant and the standard fatigue crack growth curve is obtained. In Pippan's 1994 paper [27] comparing the three test method's he obtained the following threshold results for 7020-T5.

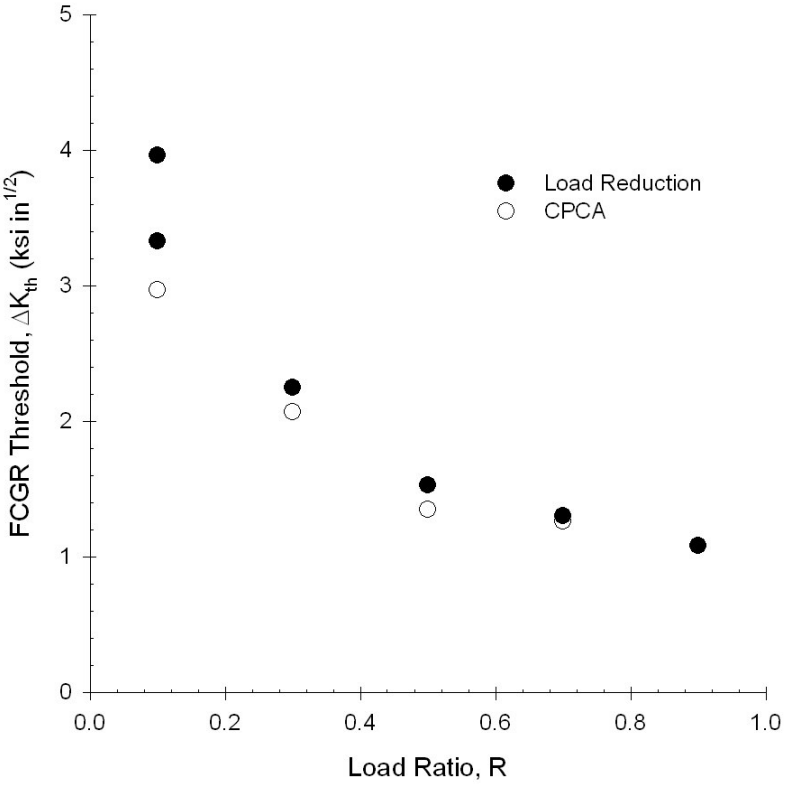

Figure 13: Comparison of threshold results for two different test methods [27].

At the lower load ratios there are large variations in threshold values, then as the load ratio increases the variations get smaller. This demonstrates the effects of closure, by which as load ratio increases the smaller the effects of closure are. Moreover, at the higher load ratios, R = 0.7, where closure is assumed to be negligible, there is a small variation in the threshold results.

There has been further research done on the CPCA method in the past few years by James et al. at NASA Langley [26, 28] and by Newman at Mississippi State [20]. James et al. has compared finite element analysis to tests performed under the CPCA test method. They have shown that the CPCA

method introduces a load history effect due to the tensile residual stress from the compression precracking of about two or three plastic zone sizes. The results of James et al.'s tests are shown in the following two figures.

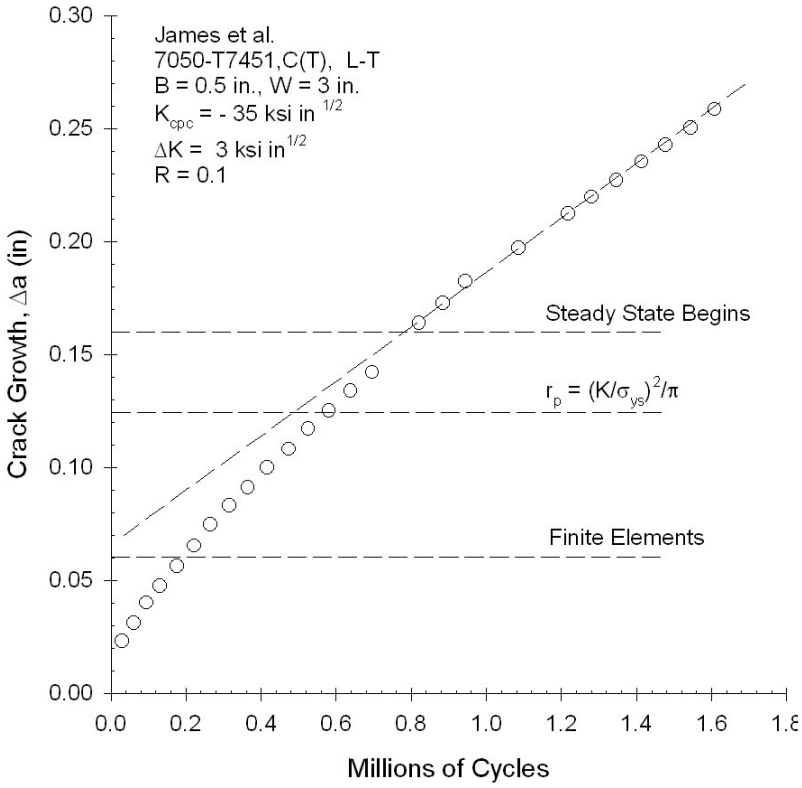

Figure 14: Residual stress effects due compression precracking [26]

Crack growth is plotted against cycles for 7050-T7451 in Figure 14. The plot exhibits the finite element and analytical plastic zone sizes and where the steady state crack growth begins. Steady state crack growth began after approximately one million cycles; this is about 4 times the finite element plastic zone cycle count and twice the Irwin plastic zone cycle count.

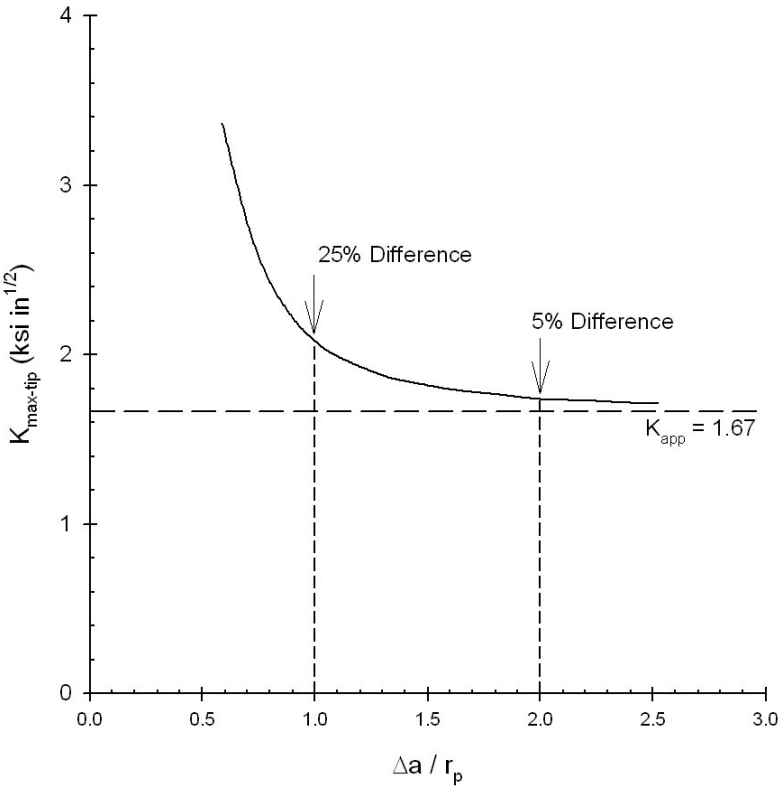

Figure 15: Difference in the applied stress and the crack tip stress during crack extension [26]

James et al then illustrate in Figure 15 that at a crack extension of approximately one plastic zone size there is about a 25% difference in the applied stress and crack tip stress. At about two plastic zone sizes the difference is only 5%.

Newman has recognized this effect, in what he refers to as the three compressive zone criteria, but shows that it has only a negligible effect on the overall fatigue crack growth curve.

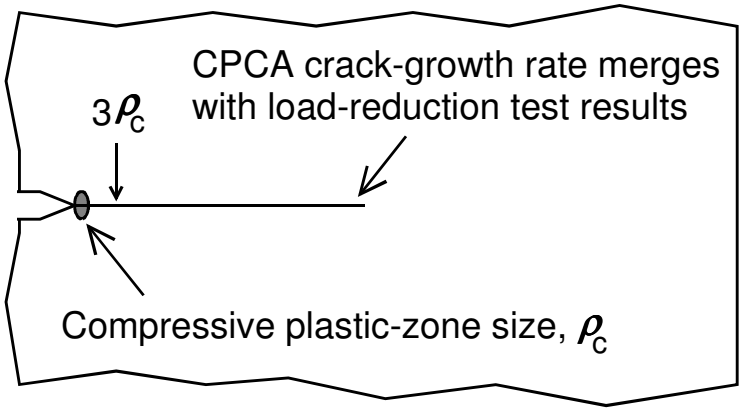

Figure 16: Three compressive plastic-zone criteria [20]

The illustration in Figure 16 illustrates to scale the point at which the two test procedures converge on a compact tension specimen. The illustration also demonstrates where the three compressive zone criteria ends, beyond which effects from compressive loading are not present. The experimental data demonstrate that the residual stress effect of three plastic zone sizes caused by the compression precracking cannot explain the variations in the lower Paris and near-threshold regime data in the load reduction and CPCA test methods. This is based on a couple of explanations:

1. The three compression plastic zone criteria is only about a sixth of the overall difference in the two procedures
2. In the early stage of crack growth, the CPCA method causes accelerated crack growth until steady state is reached (Figure 11). This is a result of the opening of the crack caused by compression precracking. The accelerated crack growth causes the crack to grow through the three compressive plastic zones near to where steady state growth begins.

CHAPTER II

ALUMINUM ALLOY 7075-T7351

The following chapter is included as a reference for the AA7075-T7351 used in fatigue crack growth testing. The chapter does not include original work by the author.

2.1 AA7075-T7351 Properties

Aluminum is one of the most abundant materials on the planet and in its pure form can be extracted from the ore bauxite. Bauxite consists of three components, aluminum, oxygen, and aluminum-oxide. After the aluminum has been extracted from the bauxite, it can then be alloyed with several different alloys such as magnesium, silicon, manganese, copper, and zinc. Through alloying pure aluminum, the ultimate tensile strength can be improved from 6-7 ksi to 40-70 ksi. The 7075 aluminum alloy, whose chemical composition is listed in Table I, is of great importance in the aerospace industry and it is the threshold behavior of this Al-Mg-Zn-Cu aluminum alloy that is the focus of this research.

Table 1

Composition of 7075-T7351 (Approx. Weight%) [29]

Zn	Mg	Cu	Cr	Fe	Si	Al
5.79	2.63	1.95	0.18	0.27	0.09	Bal.

The high strength, summarized in Table 2, comes from the formation of $MgZn_2$ precipitates during an aging heat treatment.

Table 2

Room temperature mechanical properties of 7075 aluminum alloy [29]

Alloy/Temper	Yield Strength (ksi)	UTS (ksi)	Elongation (Pct)	K_{Ic} (ksi$\sqrt{in}$)
7075-T7351	65.8	73.2	13.0	29.1

2.2 The Aging Process

The aging heat treatment consists of three steps: solution heat treatment, quenching, and aging. In the first step the material is heated to a temperature between the solvus and solidus temperatures and soaked until a homogenous solid solution state is produced within the solid microstructure. During the second step the metal in the solid solution state, is rapidly quenched to room temperature to form a supersaturated solid solution. This step is done to trap solute alloying atoms within the grain rather than letting them form an equilibrium

second phase at the grain boundaries. Finally the alloy is aged to let the solute alloying atoms form and grow second phase strengthening precipitates within the grain. The aging time and temperature affect the precipitate phase and size formed and thereby affects the strength of the alloy. The aging curve shown in Figure 17 represents the development of precipitates in the 7xxx series alloys. First Guinier-Preston (GP) Zones form which are followed by η` at the peak aged condition and finally by η precipitates in the overaged condition.

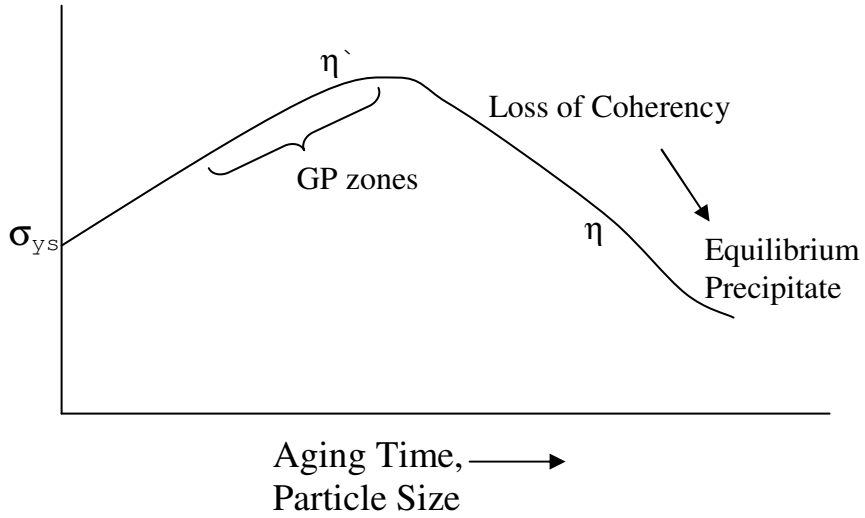

Figure 17: Variation of yield stress with aging time for an Al-Zn alloy

The precipitates formed during the under aged and peak aged conditions are coherent with the material matrix, but as aging continues there is a loss of coherency with the matrix and therefore a decrease in strength. The primary precipitate composition in 7075 is $MgZn_2$, but because of the high Cu content in 7075, the actual composition of the precipitates can range between

$Mg(Zn,Cu,Al)_2$ The variation in chemistry does not change the crystallographic structure of the precipitates [30].

2.3 Aging Heat Treatment of 7075-T7351

The 7000 series alloys are heat treatable alloys, which are aged to obtain different tempers. Of interest to this research is the overaged temper, T7351 temper. Each number in the temper designation indicates each step of the aging process that the alloy was subjected. The T7 indicates the alloy has been solution heat treated, without significant cold working, and aged in a furnace to an overaged condition. The T7 process is done to improve either stress-corrosion cracking (T73) or improve resistance to exfoliation corrosion attack (T76). The TX51 indicates a stress relief by stretching following heat treatment to reduce the amount of internal stresses. The TX51 stress relief stretching can be applied to either plate, rolled or cold-finished rod, and die or ring forgings. The post solution heat treatment stretching is applied to all fatigue critical, damage tolerant products that are aged [31].

CHAPTER III

EXPERIMENTAL DESCRIPTION

Tests were performed on Instron 8872, 5.6 kip, closed-loop servo-hydraulic load frames with digital controllers shown in Figure 18. For testing at low load ranges, 1 kip load cells were piggy backed onto the 5.6 kip load cells for higher range of accuracy. A photo of the hardware configuration is illustrated in Figure 18. For tighter tolerances on loading and compliance, the control of the testing conditions and recording crack growth was performed by Fracture Technology Associates (FTA) systems.

To measure crack growth back-face strain (BFS) gages were used and strain measurements were passed through a conditioning box into the Instron controller. This method is discussed in detail in Section 3.2. Visual measurements were taken throughout testing to corroborate the BFS readings.

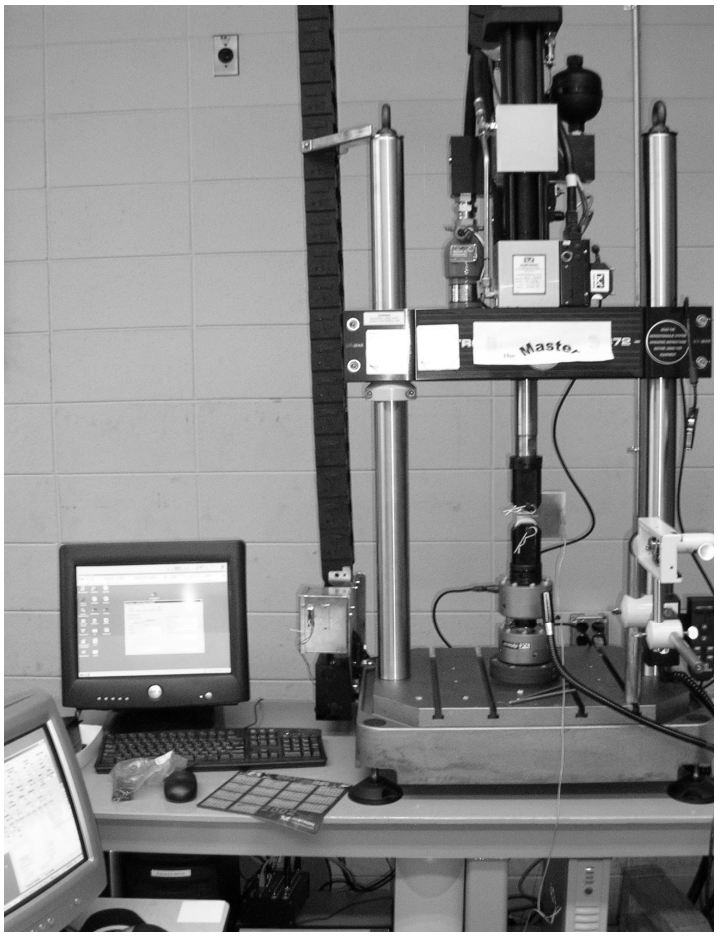

Figure 18: MSU laboratory test setup

3.1 C(T) Specimen Geometry

ASTM standard three-inch compact tension specimens, C(T), with thicknesses varying form 0.38-0.44 inches were used for fatigue testing. Two configurations of the C(T) specimen were used: a standard 3" C(T) specimen geometry with ¾" holes and an EDM notch and a modified 3" C(T) specimen with ½" holes and machined notches. The clevis grips supplied by Instron were configured with ½" pins. When using the ½" pins in the ¾" holes, the specimens

were able to rotate a fraction off the load line (up to 50 mils). The off-centered specimens were a concern because it could affect the stress intensity calibration equation, the BFS-calibration equation and the crack path. Thus the C(T) specimen geometry in Figure 19b was used with the 1/2“ holes to match the ½” pins. It was assumed that the smaller holes would not affect the K-calibration equation because the holes were machined to produce equivalent loading conditions as the standard ¾” pin holes. This assumption was verified by testing specimen T6 with the modified holes under the same conditions as specimen T1 with the standard holes. The FCGR curve for specimen T6 was identical to the FCGR curve for specimen T1.

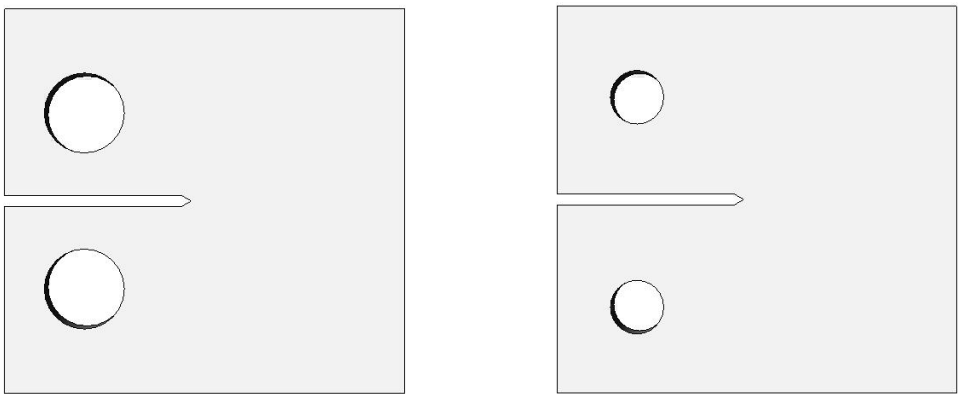

(a) (b)

Figure 19: Specimen configuration, a) standard compact tension specimen, b) modified compact tension specimen

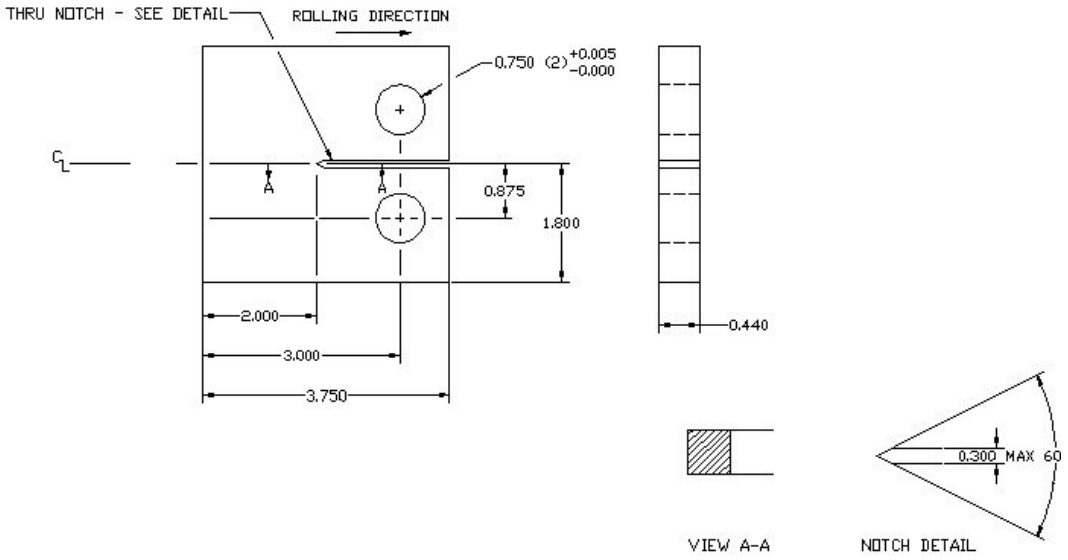

Figure 20: Standard 3" Compact tension specimen dimensions

3.2 BFS Crack Length Measurement

To measure crack length the back-face strain (BFS) compliance technique was employed. This technique uses strain gages place along the back-face of the specimen along the center of the specimen as illustrated in Figure 21.

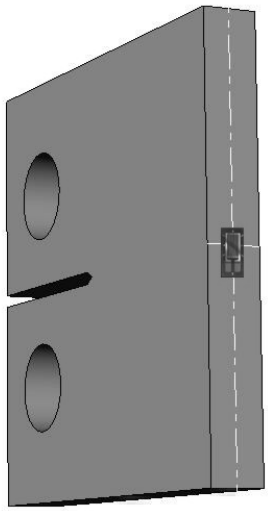

Figure 21: Location of BFS gage on compact tension specimen

Use of the BFS gage is a non-ASTM standard technique for measuring crack growth in C(T) specimens. However, the ASTM standard does present equations for BFS measurements for single edge crack tension, ESE(T), specimens. Thus a review of the literature was used to locate various equations for crack length using the BFS strain method on C(T) specimens [32, 33]. The BFS equations are summarized in Table 3, along with the crack opening displacement equation for reference.

Table 3

Back-face strain equations

Newman-Johnston (2003) [Unpublished]					
$a/W = A_0 + A_1 U + A_2 U^2 + A_3 U^3 + A_4 U^4 + A_5 U^5$					
$U = [A^{*1/2} + 1]^{-1}$			$A^* = \lvert\varepsilon EBW/P\rvert$		
A0 = 1.0343	A1 = -2.8098	A2 = 4.1335	A3 = -23.6937	A4 = 76.371	A5 = -83.25
Riddell-Piascik (1998) [32]					
$a/W = A_0 + A_1 (\log A^*) + A_2 (\log A^*)^2 + A_3 (\log A^*)^3 + A_4 (\log A^*)^4 + A_5 (\log A^*)^5$					
$A^* = \lvert\varepsilon EBW/P\rvert$					
A0 = -0.07978	A1 = 0.83982	A2 = -0.64978	A3 = 0.53227	A4 = -0.21704	A5 = 0.03154
Maxwell (1987) [33]					
$a/W = A_0 + A_1 U + A_2 U^2 + A_3 U^3 + A_4 U^4 + A_5 U^5 + A_6 U^6$					
$U = [A^{*1/2} + 1]^{-1}$			$A^* = \lvert\varepsilon EBW/P\rvert$		
A0 = 0.99999	A1 = -2.00085	A2 = 0.75959	A3 = 10.01565	A4 = -18.39149	A5 =14.23767
A6 = -4.05333					
COD [4]					
$a/W = A_0 + A_1 U + A_2 U^2 + A_3 U^3 + A_4 U^4 + A_5 U^5$					
$U = [A^{*1/2} + 1]^{-1}$			$A^* = \lvert\nu EB/P\rvert$		
A0 = 1.0012	A1 = -4.9165	A2 = 23.057	A3 = -323.91	A4 = 1798.3	A5 = -3513.2

In the equations A* represents the compliance, a unit less parameter. A comparison of compliance to a/W is presented in the Figure 22.

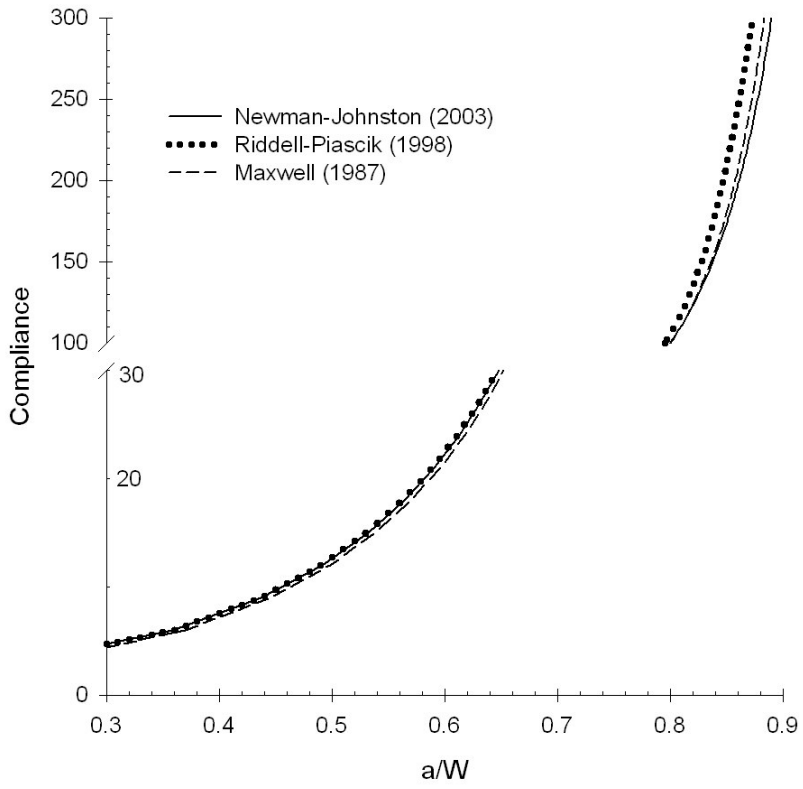

Figure 22: Comparison of Newman-Johnston, Riddell-Piascik, and Maxwell BFS equations

The Maxwell equation displays a high percent difference at the low a/W ratios as shown in Figure 23. The Newman-Johnston and Riddell-Piascik equations exhibit values within 0.5% of each other up to an a/W ratio of approximately 0.8. The Newman-Johnston equation was chosen because of its similarity to the COD equation; allowing easy implementation into the FTA system software. The FTA system is setup for either COD compliance or electric potential drop. The Newman-Johnson equation contains the same number of constants and the same equation for the variable U. The only difference is the

width is included in the BFS compliance equation. Therefore when setting up FTA for testing the width must be included in the BFS calibration factor.

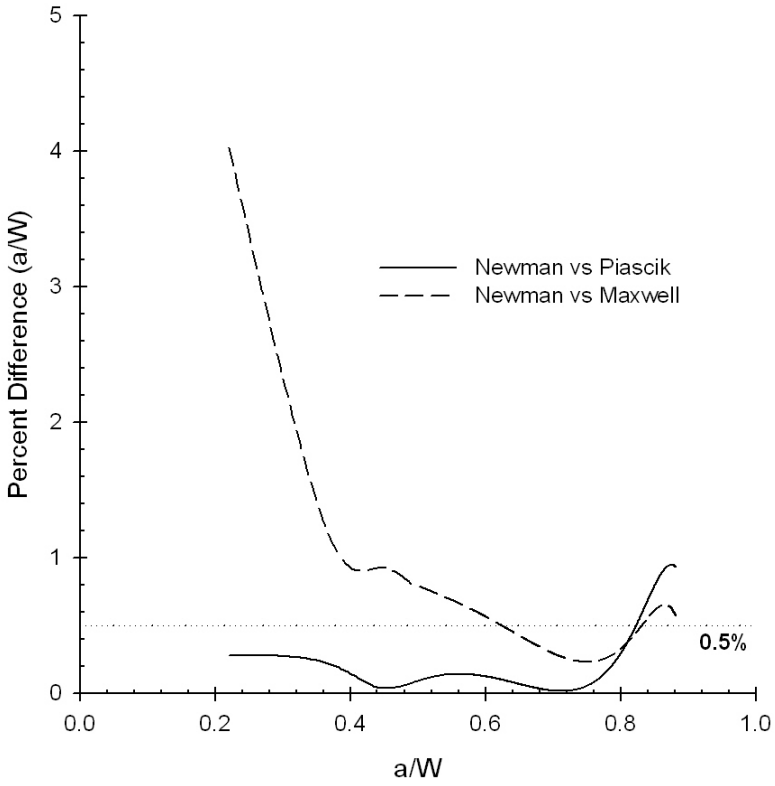

Figure 23: Percent difference between BFS equations

3.3 Compression-Compression Precracking Method

Two different methods of performing compression-compression tests were compared to find the most effective way to obtain compression precracks. The first method was to load the bottom of the pin holes, similar to the technique used to test in tension. This method was found to cause the specimen to fracture along the load line. The second method compared, shown in Figure 24, was to

fix metal platens to the top of the specimen along the load line, then using the 2" clevises the specimen was loaded.

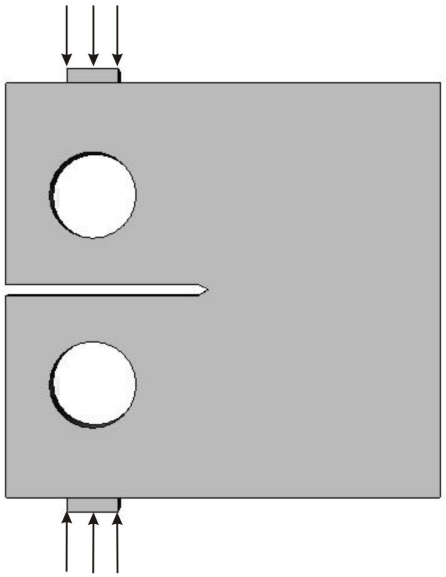

Figure 24: Loading of C(T) specimen under compression

This method was found to give accurate, repeatable results.

3.4 Constant Amplitude Fatigue Crack Growth Test

Constant-amplitude loading allows for natural steady state loading free from testing influences. A difficulty in the CPCA test method though is choosing a starting stress-intensity range. Numerous cycles can be applied below the true threshold value because the threshold is attained from below. Therefore, the threshold must be reached through a trial and error approach. Loading is started low and cycled for several million cycles, and then stepped up until steady crack

growth is obtained. Newman's FASTRAN program was utilized to assist in selecting a starting point for CPCA testing.

Constant amplitude loading was per ASTM E647-00. Prior to testing visual measurements were made for thickness, width, and crack length for the FTA program. This allows the program to calculate the stress intensity and gives it a starting point for the crack length.

CHAPTER IV

RESULTS AND DISCUSSION

A test program was executed to obtain threshold and near-threshold results for aluminum alloy 7075-T7351, using the compression pre-cracking constant-amplitude (CPCA) threshold testing method. Compact tension specimens were tested under load ratios (R) of 0.1, 0.4, and 0.7. Results were compared with data that were generated using the load-reduction procedures.

4.1 Precracking

The following conditions were applied during compression precracking. Precrack loads were based on earlier tests on 7075-T651 and 2324-T351. The initial goal was to obtain a sharp precrack to precipitate crack growth while getting away from notch effects. Then as more research was done into the three compressive criteria it was decided to try to reduce the precrack length, thus reducing size of the compressive plastic zone. The rationale for the decision was based on some research by Pippan. In the same study as shown in Figure 13, two specimens were precracked under compression-compression to lengths of

12 mils and 4 mils, then fatigue tested under constant amplitude loading. There was no difference found in threshold results. Likewise two specimens were precracked under tension-tension to lengths of 118 mils and 40 mils and then load shedded to threshold and two different thresholds were found as shown in Figure 13.

Table 4

Results of precracking

Specimen #	Pmax (lbf)	Pmin (lbf)	Number of Cycles	Frequency (Hz)	Precrack Δa (mils)	Final K_{max} (ksi $in^{1/2}$)	Strength Ratio R_{sc}
T1	-2600	-100	2,500,000	10	20.1	-23.9	-0.31
T3	-2600	-100	2,500,000	15	17.9	-23.9	-0.31
T5	-2600	-100	2,500,000	15	16.8	-23.8	-0.31
T6	-2200	-100	2,500,000	15	9.5	-19.8	-0.30
T7	-2200	-100	2,500,000	15	9.9	-19.6	-0.30
T8	-1800	-100	2,500,000	15	5.2	-15.9	-0.25

The ASTM standard E399-90 for plane strain fracture toughness promotes for early crack initiation the use of a compressive load applied, prior to precracking [34]. The compressive load must not allow the specimen strength ratio to exceed -1. The specimen strength ratio is the ratio of the nominal section stress, at maximum load, to the yield strength. The specimen strength ratio is defined for a compact tension specimen as,

$$R_{sc} = \frac{2P_{\max}(2W + a)}{B(W - a)^2 \cdot \sigma_{ys}} \tag{9}$$

where P_{max} is the maximum load, W is the width, B is the thickness, a is crack length, and σ_{ys} is the yield strength. Although, the specimen strength ratio is not defined in the ASTM E647-00 it is a good parameter to check for yielding when precracking under compression-compression. The specimen strength ratio has been calculated, in Table 4, for the 6 specimens tested using the CPCA approach. All six specimens are below a third of the compressive yield.

The fracture surface for specimen T1 is shown in Figure 25. On the right is the notch, then the small compressive precracking zone can be observed stemming from the notch, then the constant amplitude fatigue surface, followed by the fracture surface to the left. The compression precracking yields a flat fracture surface formed as shown in Figure 25, with the crack length approximately equal across the width of the precrack

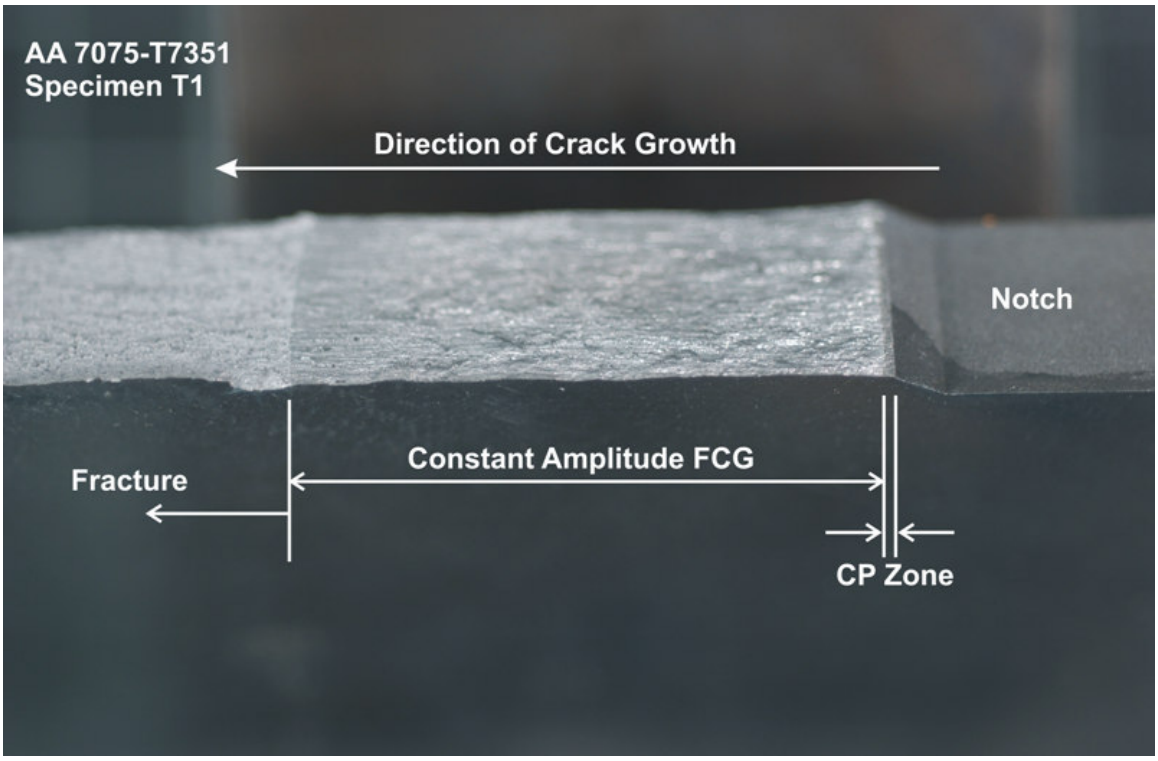

Figure 25: Specimen fracture surface

4.2 Test Matrix

A total of six tests were performed using the compression-compression constant amplitude test method. Three tests were performed at a load ratio of 0.1, two at a load ratio of 0.4, and one at a load ratio of 0.7. Lower load ratios were tested to identify the effects of closure. Conditions under which tests were performed are shown in Table 5.

Table 5

Constant amplitude testing parameters

Specimen #	Load Ratio	Freq (Hz)	Pmax (lbf)	Initial ΔK (ksi $in^{1/2}$)	Final ΔK (ksi $in^{1/2}$)
T1	0.1	20	250	2	6.88
T3	0.7	20	470	1.15	7.13
T5	0.4	20	300	1.55	6.87
T6	0.1	20	250	2.1	5.04
T7	0.1	20	200	1.6	7.81
T8	0.4	20	250	1.35	4.06

Only one test was performed at a load ratio of 0.7. The resultant fatigue crack growth curve is shown in Figure 26.

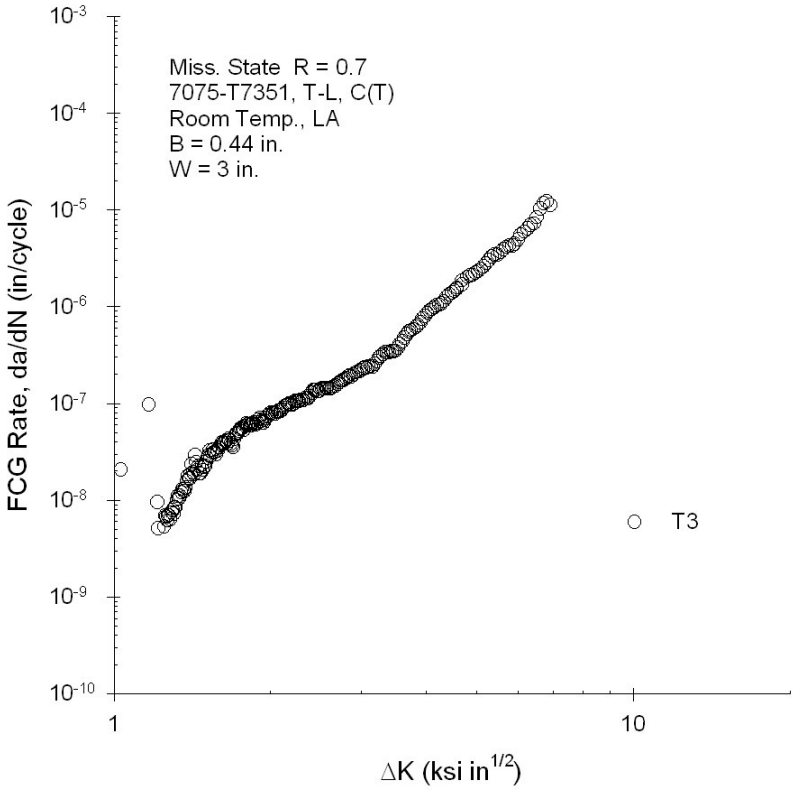

Figure 26: Fatigue crack growth curve for R = 0.7

Two tests were performed at the load ratio of 0.4. The first test, T5, was started at a high ΔK to get an idea of the shape of the fatigue crack growth curve. The subsequent test, T8, was started lower to get more of the near-threshold region.

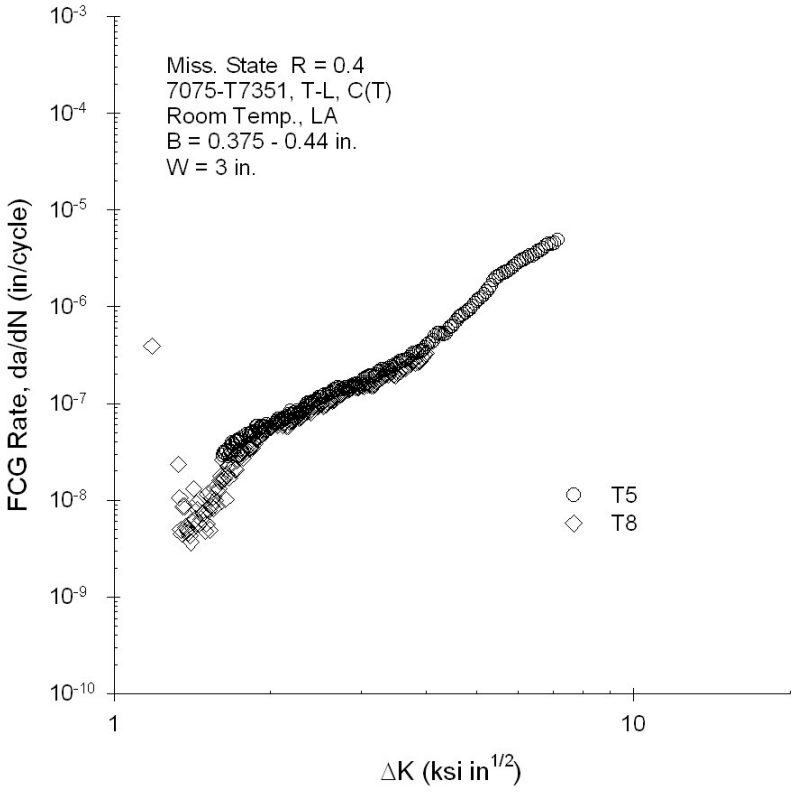

Figure 27: Fatigue crack growth curve for R = 0.4

Three tests were performed at the load ratio of 0.1. Like T5, specimen T1 was performed to get an idea of the shape of the fatigue crack growth curve. Specimen T6 was the first specimen with the modified hole geometry. It was started at the same conditions as T1 to verify that the new geometry had no effect on the fatigue crack growth properties. The last test, T8, was started lower to get obtain more of the near-threshold region.

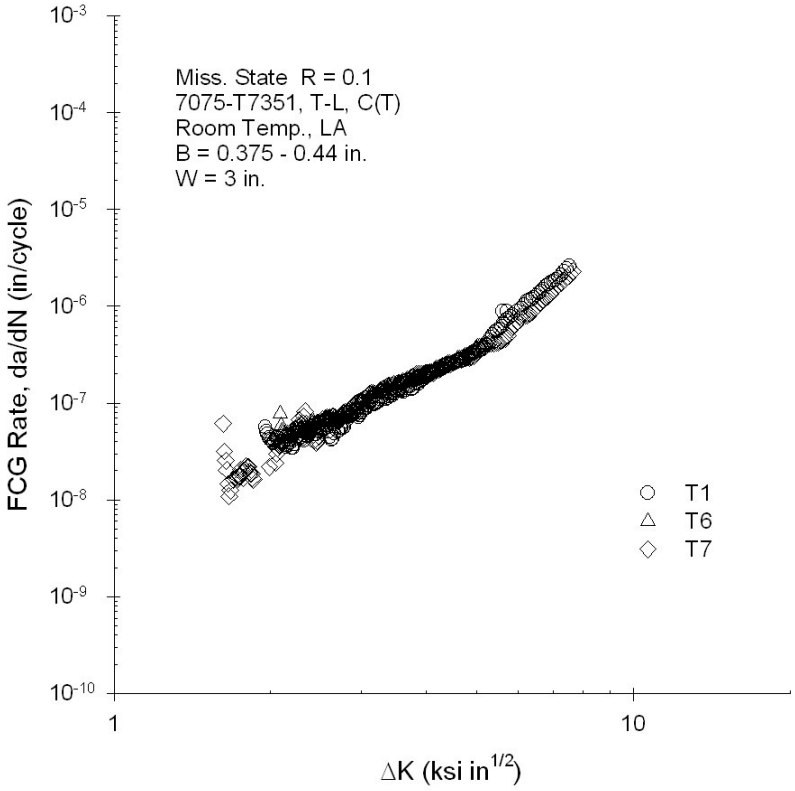

Figure 28: Fatigue crack growth curve for R = 0.1

4.3 Discussion of CPCA Test Method Results

Load reduction data from Figure 9, were used to compare and contrast the two test methods. Both sets of data are from 7075-T7351 in the TL orientation with similar thicknesses and widths. The two loading methods at a load ratio of 0.7 are shown in Figure 29. The two test methods yield very similar results as was expected at the higher load ratios. There is a slightly lower threshold for the CPCA procedure but more testing is needed to discern if this is an actual artifact of the testing procedure.

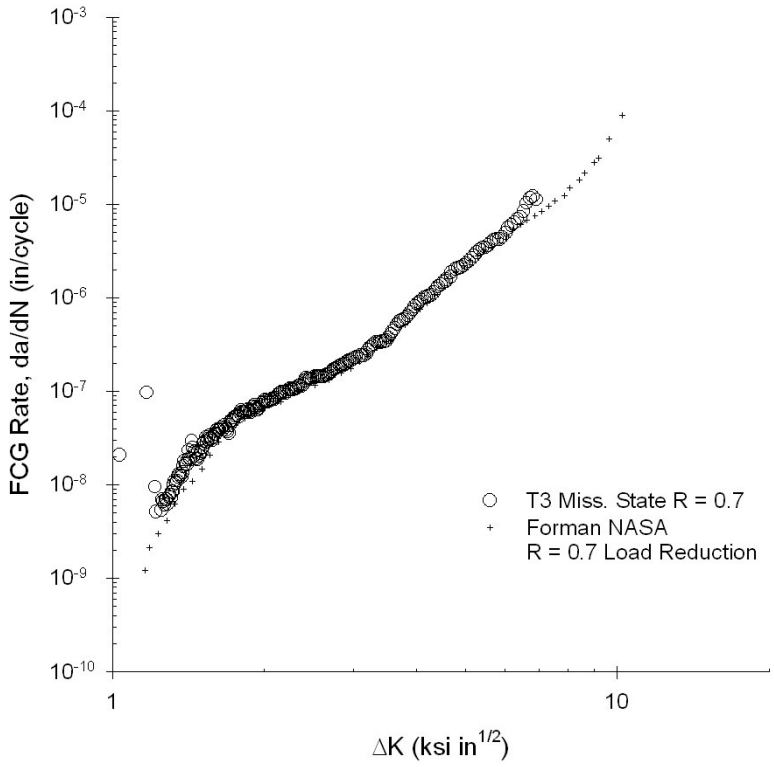

Figure 29: Comparison of load reduction and CPCA data at R = 0.7

FCG data at a load ratio of 0.4 are illustrated in Figure 30. The R of 0.7 load reduction test is included for reference. The CPCA near-threshold data follows along the R of 0.7 data, and then at the Paris regime the data follows the path of the R of 0.4 load reduction data.

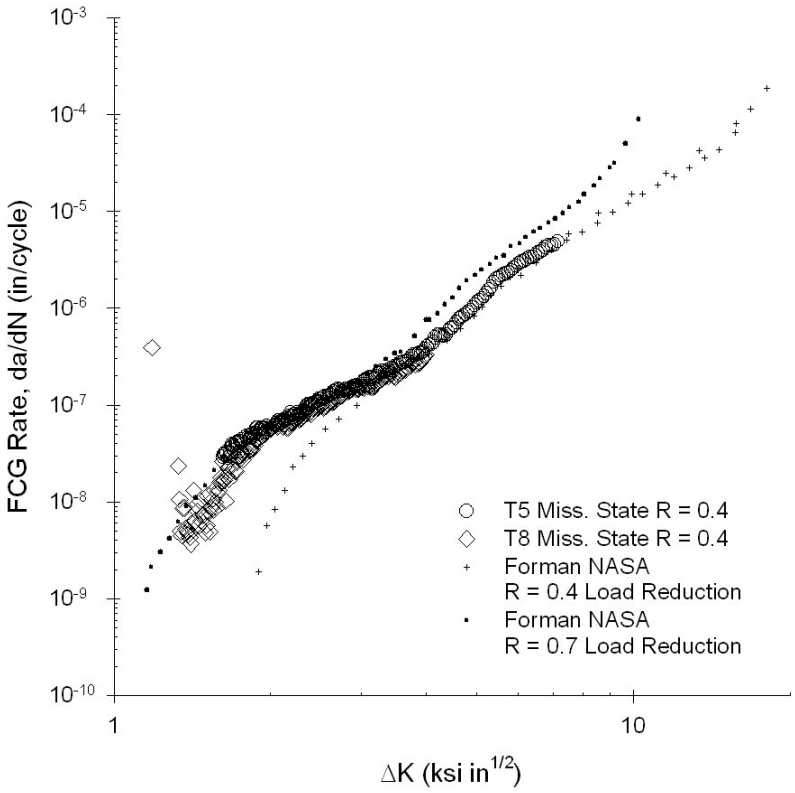

Figure 30: Comparison of load reduction and CPCA data at R = 0.4

The load ratio data of 0.1 is shown in Figure 31. Again the load ratio data of 0.7 is shown for reference. The data from the three CPCA tests follow along just slightly to the right of the R of 0.7 data. The data provides evidence for the load history effects caused by the load reduction procedure. The lower load ratios tested under the load reduction procedure exhibit lower crack growth rates due to the reduction in the applied stress intensity range caused by closure. Whereas the CPCA data exhibits steady state crack growth throughout the FCGR curve.

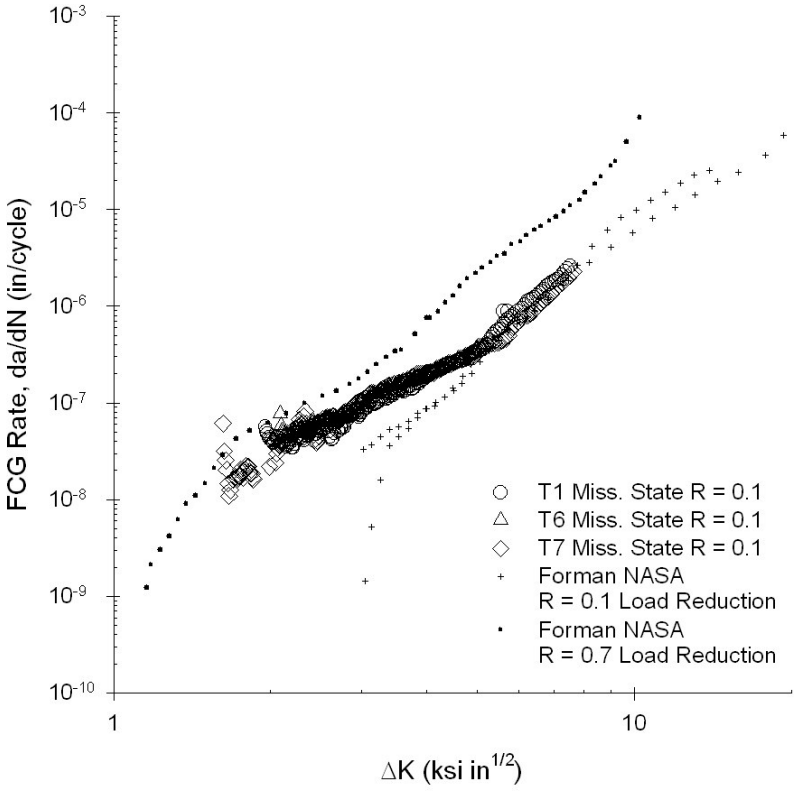

Figure 31: Comparison of load reduction and CPCA data at R = 0.1

The CPCA data displays a number of consistent trends. The lower load ratios seem to follow along the high load ratios until approximately a crack growth rate of $4x10^{-8}$ in/cycle. There is then a transition period where the data ultimately converges on the conventional load reduction data at an approximate FCG rate of $4x10^{-7}$ in/cycle, where it continues along the conventional FCG curve. Where the two curves converge is the same point at which conventional load shedding is initiated going down the curve and constant amplitude is initiated going up the curve. Again, this supports that the load shedding procedure introduces a "load history" effect that has an adverse impact on subsequent fatigue crack growth.

Another trend displayed in the CPCA data are the initial high growth rates at the start of constant amplitude testing. The compression precracking leaves the crack open. As a result, the natural steady state plasticity must build up at the crack tip prior to reaching steady state. In addition the compression precracking leaves tensile residual stresses that initially drive crack growth until crack opening stresses are stabilized and steady crack growth is reached. This has been shown to be 2-3 compressive plastic zone sizes.

The above data were spine fitted and stress intensity factor ranges were determined from Forman's load reduction data at the fatigue crack growth rate threshold, $4x10^{-9}$ in/cycle, and at the crack growth rate at which ASTM standard load shedding is initiated, $4x10^{-7}$ in/cycle (Figure 32). Fatigue crack growth rates were then determined for the CPCA at the same stress intensity factor ranges.

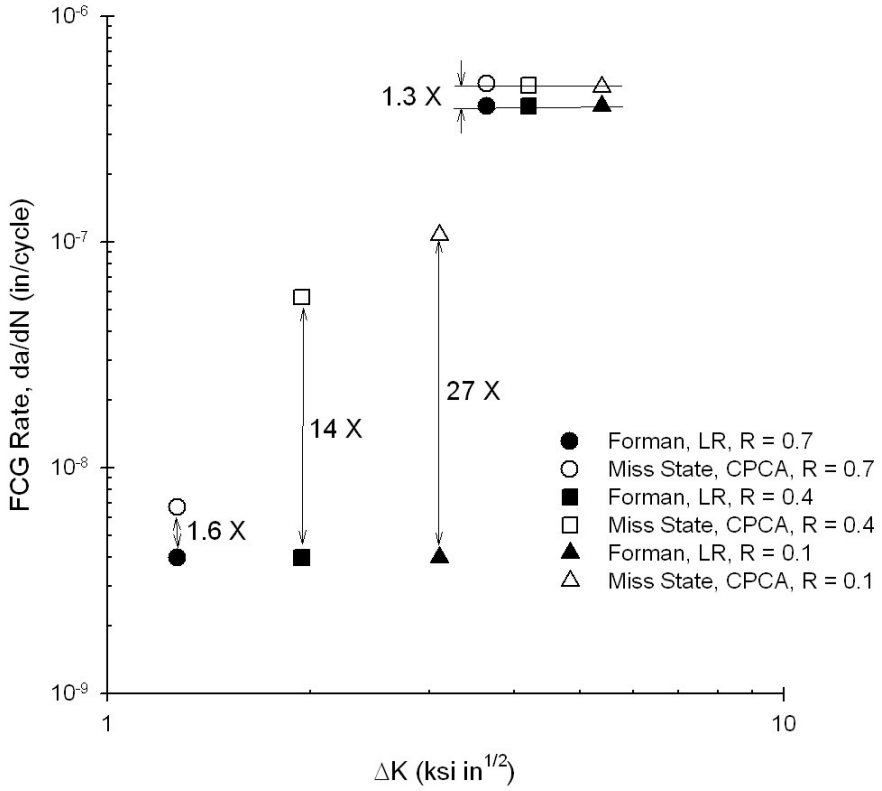

Figure 32: Comparison of FCG rates for load reduction and CPCA test procedures

At an applied ΔK of 1.27ksi-√in at a load ratio of 0.7, the CPCA method produces growth rates of approximately 1.6 times the load reduction procedure. This is not a large difference considering the many variables that can affect ΔK at threshold. For a load ratio of 0.4, the threshold stress intensity factor range was determined for the load reduction procedure to be 1.94ksi-√in. At the same stress intensity factor range, using the CPCA procedure, the crack growth rate is 14 times higher than the fatigue crack growth rate threshold. Likewise, at a load ratio of 0.1, the threshold stress intensity factor range was determined for the load reduction procedure to be 3.10ksi-√in. At the same stress intensity factor

range, using the CPCA procedure, the fatigue crack growth rate is 27 times higher than the ASTM fatigue crack growth threshold. The higher growth rates are included in Figure 32 to demonstrate approximately where the two test procedures converge.

A literature review was performed to obtain FCGR threshold results for AA7075-T7351 from various labs under similar testing and material conditions. In addition to the data obtained from Forman et al. [17], threshold data were also found from Suresh et al. [29], Stanzl-Tschegg et al. [35], and Holper et al. [36]. A comparison of some of the conditions under which the test were performed is shown in Table 6. All the tests apart from those performed at Mississippi State, were performed under the load reduction procedure.

Table 6

Comparison of FCGR testing conditions

Reference	Material	Product Form	Spec. Config.	Orient.	Temp (F)	RH (%)	B (in)	W (in)
Miss. State	7075-T7351	Plate	C(T)	T-L	RT	LA	.380-0.44	3
Forman	7075-T7351	Plate	C(T)	T-L	70	LA	0.455	3
Suresh [29]	7075-OA	-	C(T)	L-T	RT	95	0.25	-
Stanzl [35]	7075-OA	Plate	C(T)	-	RT	LA	0.394	2.36
Holper [36]	7075-T7351	.79" Sheet	M(T)	T-L	68	40-60	0.197	0.785

The FCGR threshold results are compared in Figure 33. While the lower load ratios show widely scattering threshold data, the CPCA threshold results provide a lower bound for FCGR threshold.

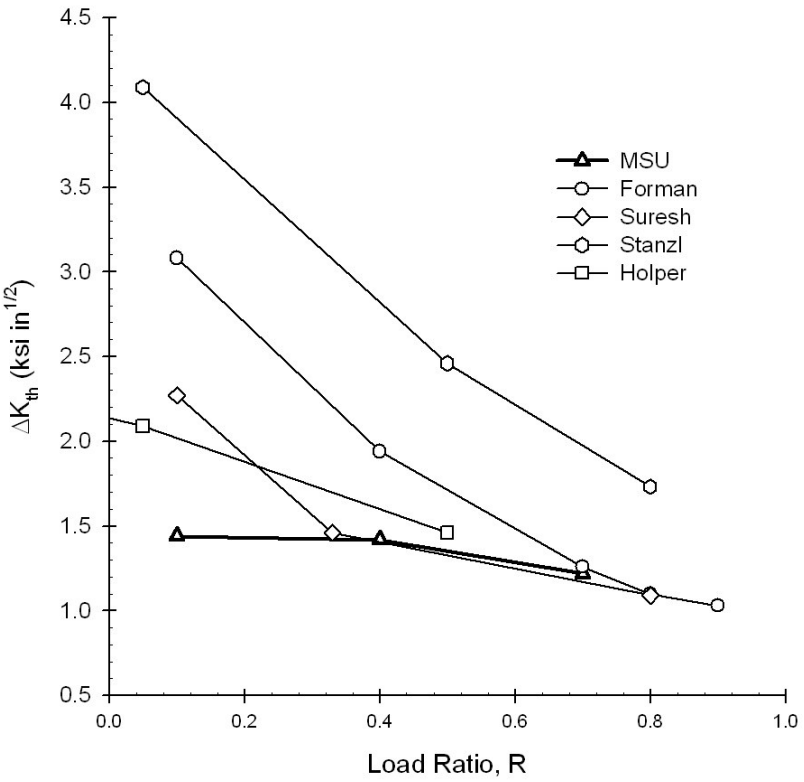

Figure 33: Comparison of FCGR thresholds from literature

The goal of the ASTM standard E647-00 with regard to threshold is to provide a lower bound for which cracks will not propagate. The current load reduction procedure does not achieve this intention. Ideally the FCGR threshold should be a unique property based on the material, load ratio, and environment. The above comparison clearly shows that this is not the case even under the same ASTM load reduction procedure.

CHAPTER V

SUMMARY

The load history effects sustained from the load shedding test method has been shown to cause higher thresholds than steady state conditions. Therefore, a new procedure to obtain fatigue crack growth rate data has been proposed to minimize these effects. In this procedure the specimen is precracked under compression. This allows for testing to be performed under constant amplitude loading throughout the three stages of fatigue crack growth for long cracks: threshold, Paris regime, and fracture.

In the present study tests were performed under three load ratios (0.1, 0.4, and 0.7) using aluminum alloy 7075-T7351. The high load ratio, R = 0.7, was tested to show the minimal effects of plasticity induced closure at the high load ratios. The lower load ratios, R = 0.4 and 0.1, showed significantly lower threshold and near- threshold stress intensity values, whereas values were similar at R = 0.7.

The load shedding data demonstrated higher levels of closure due to the dropping of loads above threshold. As a result of closure unique values of FCGR threshold for material, load ratio, and environment proves nearly impossible. The

CPCA method offers an alternative approach to generate lower-bound near-threshold data. With time and a broader application and use by the scientific community the value of this approach will be established.

REFERENCES

1. Stephens, R.I., Fatemi, A., Stephens, R.R., and Fuchs, H.O., *Metal Fatigue in Engineering*. 2 ed. 2001, New York: Wiley.

2. Paris, P.C., Gomez, M.P., and Anderson, W.E., "A Rational Analytical Theory of Fatigue"*. Trend Eng.*, 1961. **13**(9): p. 9.

3. Grandt, A.F. Jr., *Fundamentals of Structural Integrity: Damage Tolerant Design adn Nondestructive Evaluation*. 2004, Hoboken: Wiley.

4. "E647-00 Standard Test Method for Measurement of Fatigue Crack Growth Rates", *Annual Book of ASTM Standards: Metals Test Methods and Analytical Procedures*. 2003, ASTM. p. 615-657.

5. Carter, R.D., Lee, E.W., Starke, E.A. Jr., and Beevers, C.J., "The Effect of Microstructure and Environment on Fatigue Crack Closure of 7475 Aluminum Alloy"*. Metallurgical Transactions A*, 1984. **15A**: p. 555-563.

6. Elber, W., "Fatigue Crack Closure Under Cyclic Tension"*. Engineering Fracture Mechanics*, 1970. **2**: p. 37-45.

7. Newman, J.C. Jr., "Analyses of Fatigue Crack Growth and Closure Near Threshold Conditions for Large-Crack Behavior", *Fatigue Crack Growth Thresholds, Endurance Limits, and Design*. 2000, American Society for Testing and Materials: ASTM STP 1372. p. 227-251.

8. Vasudevan, A.K., Sadananda, K., and Louat, N., "A review of crack closure, fatigue crack threshold and related phenomena"*. Materials Science and Engineering*, 1994. **A188**: p. 1-22.

9. Suresh, S., Zamiski, G. F., and Ritchie, R. O., "Oxide-Induced Closure: An Explanation for Near-Threshold Corrosion Fatigue Crack Growth Behavior"*. Metallurgical Transactions A*, 1981. **12A**: p. 1435-1443.

10. Suresh, S. and Ritchie, R. O., "A Geometric Model for Fatigue Crack Closure Induced by Fracture Surface Roughness"*. Metallurgical Transactions A*, 1982. **13A**: p. 1627-1631.

11. McClung, R.C., "Analysis of Fatigue Crack Closure During Simulated Threshold Testing". 2000, American Society for Testing and Materials: ASTM STP 1372. p. 209-226.

12. Liknes, H.O. and Stephens, R.R., "Effect of Geometry and Load History on Fatigue Crack Growth in Ti-6222", *Fatigue Crack Growth Thresholds, Endurance Limits, and Design*. 2000, American Society for Testing and Materials: ASTM STP 1372. p. 175-191.

13. Forth, S.C., Newman, J.C. Jr., and Forman, R.G., "Anomalous Fatigue Crack Growth Data Generated Using ASTM Standards"*. Journal of Testing and Evaluation*, 2005.

14. Garr, K.R. and Hresko, G.C. III, "A size effect on the Fatigue Crack Growth Rate Threshold of Alloy 718", *Fatigue Crack Growth Thresholds, Endurance Limits, and Design*. 2000, American Society for Testing and Materials: ASTM STP 1372. p. 155-174.

15. Pippan, R., Riemelmoser, F.O., Weinhandl, H., and Kreuzer, H., "Plasticity-Induced Crack Closure Under Plane-Strain Conditions in the Near-Threshold Regime"*. Philosophical Magazine A*, 2002. **82**(17/18): p. 3299-3309.

16. Bush, R. W., Donald, J. K., and Bucci, R. J., "Pitfalls to Aviod in Threshold Testing and its Interpretation", *Fatigue Crack Growth Thresholds, Endurance Limits, and Design*. 2000, American Society for Testing and Materials: ASTM STP 1372. p. 269-284.

17. Forth, S.C., Newman, J.C. Jr., and Forman, R.G., "Evaluation of Fatigue Crack Thresholds Using Various Test Methods." *Fatigue and Fracture Mechanics*. 2002, ASTM STP 1417: 33.

18. Newman, J.C. Jr., Brot, A., and Matias, C., "Crack-growth calculations in 7075-T7351 aluminum alloy under various load spectra using an improved crack-closure model"*. Engineering Fracture Mechanics*, 2004. **71**: p. 2437-2363.

19. Newman, J.C. Jr, "A Crack-Closure Model for Predicting Fatigue Crack Growth under Aircraft Spectrum Loading", *Methods and Models for Predicting Fatigue Crack Growth under Random Loading*. 1981, American Society for Testing and Materials: ASTM STP 748. p. 53-84.

20. Newman, J.C. Jr., Schneider, J.A., Daniels, C.A., and McKnight, D.H. "Compression Pre-cracking to Generate Near Threshold Fatigue Crack Growth Rates in Two Aluminum Alloys*".International Conference on Fatigue Damage of Structural Materials*. Hyannis, Ma: 2004.

21. Forth, S.C., Newman, J.C. Jr., and Forman, R.G., "On Generating Fatigue Crack Growth Thresholds"*. International Journal of Fatigue*, 2003. **25**: p. 9-15.

22. Suresh, S., "Crack Initiation in Cyclic Compression and its Applications "*. Engineering Fracture Mechanics*, 1985. **21**: p. 453-463.

23. Christman, T. and Suresh, S., "Crack Initiation Under Far-Field Cyclic Compression and the Study of Short Fatigue Cracks "*. Engineering Fracture Mechanics A*, 1986: p. 953-964.

24. Pippan, R., Plochl, L., Klanner, F., and Stuwe, H.P., "The use of fatigue specimens precracked in compression for measuring threshold values and crack growth"*. Journal of Testing and Evaluation*, 1994. **22**: p. 98-103.

25. Hubbard, R.P., "Crack Growth Under Cyclic Compression"*. Journal of Basic Engineering*, 1969. **91**: p. 625-631.

26. James, M.A., Forth, S.C., and Newman, J.A. "Load History Effects Resulting from Compression Precracking*".Fatigue and Fracture Mechanics*. ASTM 1461. West Conshohocken, PA: 2004.

27. Pippan, R. and Stuwe, H.P., "A Comparison of Different Methods to Determine the Threshold of Fatigue Crack Propagation "*. International Journal of Fatigue*, 1994. **16**(8): p. 579-582.

28. James, M.A., Forth, S.C., Johnston, W.M., Newman, J.A., and Everett, R.A., "Effects of Compression Precracking on Subsequent Crack Growth"*. ECF*, 2004. **15**.

29. Suresh, S., Vasudevan, A.K., and Bretz, P.E., "Mechanisms of Slow Fatigue Crack Growth in HIgh Strength Aluminum Alloys: Role of Microstructure and Environment"*. Metallurgical Transactions A*, 1984. **15A**: p. 369-379.

30. Dieter, G.E., *Mechanical Metallury*. 3rd ed. 1986, Boston: McGraw Hill.

31. Kaufman, G.J., *Introduction to Aluminum Alloys and Tempers*. 2000, Materials Park, OH: ASM International.

32. Riddell, W.T. and Piascik, R.S., "A Back-Faced Strain Compliance Expression for the Compact Tension Specimen". *Journal of Testing and Evaluation*, 1999. **27**(2): p. 167-170.

33. Maxwell, D. C., *Strain Based Compliance Method for Determining Crack Length for a CT Specimen*, in *Airforce Interim Report*. 1987, Air Force Wright Aeronautical Laboratories.

34. "E399-90 Standard Test Method for Plane-Strain Fracture Toughness of Metallic Materials", *Annual Book of ASTM Standards: Metals Test Methods and Analytical Procedures*. 2003, ASTM. p. 451-482.

35. Stanzl-Tschegg, S.E., Plasser, O., Tschegg, E.K., and Vasudevan, A.K., "Influence of Microstructure and Load Ratio on Fatigue Threshold Behavior in 7075 Aluminum Alloy". *International Journal of Fatigue*, 1999. **21**: p. S255-S262.

36. Holper, B., Mayer, H., Vasudevan, A.K., and Stanzl-Tschegg, S.E., "Near Threshold Fatigue Crack Growth at Positive Load Ratio in Aluminum Alloys at Low and Ultrasonic Frequency: Influences of Strain Rate, Slip Behaviour, and Air Humidity". *International Journal of Fatigue*, 2004. **26**: p. 27-38.